Full Paper

Journal of the Brazilian Chemical Society

https://dx.doi.org/10.21577/0103-5053.20260003

*J. Braz. Chem. Soc.* **2026**, *37*, e-20260003, 1-23


# Enhanced Catalysis of Ibuprofen Esterification by CALB Immobilized on Functionalized Magnetic Nanoparticles

***Juliana F. Serpa,*** [a] ***Pierre B. A. Fechine,*** [b] ***Luciana R. B. Gonçalves,*** [c] ***Aluisio M. da Fonseca,*** [a] ***Jesús Fernández-Lucas,*** [d,e,f] ***José Cleiton S. dos Santos*** [a] ***and Maria Cristiane M. de Souza*** [*,a]

[a]*Instituto de Engenharias e Desenvolvimento Sustentável (IEDS), Universidade da Integração Internacional da Lusofonia Afro-Brasileira (UNILAB), Campus das Auroras, Rua José Franco de Oliveira, s/n, Zona Rural, Redenção 62790-970 Itapajé-CE, Brazil*

[b]*Departamento de Química Analítica e Físico-Química, Universidade Federal do Ceará (UFC), Campus do Pici, Bloco 940, Av. Humberto Monte, 2825, 60455-760 Fortaleza-CE, Brazil*

[c]*Departamento de Engenharia Química, Universidade Federal do Ceará (UFC), Campus do Pici, Bloco 709, Av. Humberto Monte, 2825, 60455-760 Fortaleza-CE, Brazil*

[d]*Applied Biotechnology Group, Universidad Europea de Madrid, Urbanización El Bosque, 28670, Villaviciosa de Odón (Madrid), Spain*

[e]*Grupo de Investigación en Ciencias Naturales y Exactas, GICNEX, Universidad de la Costa, CUC, Calle 58 No. 55-66, 080002 Barranquilla, Colombia*

[f]*Department of Biochemistry and Molecular Biology, Faculty of Biology, Universidad Complutense de Madrid, C. de José Antonio Novais, 12, 28040, Madrid, Spain*

This study investigates the performance of lipase B from *Candida antarctica* (CALB) immobilized on magnetic $Fe_3O_4$ nanoparticles (MNs) for the enantioselective esterification of racemic ibuprofen. The nanoparticles were synthesized by co-precipitation and subsequently functionalized with γ-aminopropyltriethoxysilane (APTS) and glutaraldehyde (GLU) to provide reactive aldehyde groups for enzyme attachment. CALB was covalently immobilized onto the activated support, and the resulting biocatalyst was characterized by X-ray diffraction (XRD) and Fourier-transform infrared spectroscopy (FTIR), confirming successful functionalization and enzyme immobilization. The effects of stirring speed (20-250 rpm), enzyme loading (50-650 U *p*-nitrophenyl butyrate (*p*-NPB) $g^{-1}$), contact time (0.5-5 h), glutaraldehyde concentration (2.5-25%), and sodium dodecyl sulfate (SDS, 0.23%) addition were systematically evaluated. The optimal immobilization conditions (45 rpm, 25 °C, pH 7.0, and 1 h of contact with an enzyme load of 80 U *p*-NPB $g^{-1}$) yielded an immobilization efficiency of 53% and an immobilized enzyme activity of 29.1 U $g^{-1}$. The MNs-CALB derivative exhibited excellent thermal stability (20-fold higher half-life than the soluble enzyme) and was successfully applied in the esterification of racemic ibuprofen with 1-propanol in cyclohexane, preferentially producing the (*R*)-(−)-ibuprofen propyl ester. Molecular docking simulations supported these results by demonstrating favorable interactions between the (*R*)-enantiomer and CALB's catalytic triad (Ser105-His224-Asp187). These findings highlight the potential of magnetically recoverable nanobiocatalysts as efficient, stable, and enantioselective systems for green and sustainable synthesis of chiral pharmaceuticals.

**Keywords:** lipase, immobilization, biocatalysts, ibuprofen, docking studies

*e-mail: mariacristiane@unilab.edu.br
Editor handled this article: Juliano Alves Bonacin (Associate)

## Introduction

Lipases produced by *Candida* sp. are well-established enzymes for biocatalysis, especially lipase B from *Candida antarctica* (CALB).[1] CALB has been studied for potential applications in the food, detergent, pharmaceutical, textile, cosmetic, paper, and oleochemical industries.[2,3] These applications are possible due to the wide range of specificity for substrates, high activity under mild reaction conditions, stability against organic solvents, high thermal and pH stability, and stereospecificity of lipases.[4,5]

Unlike other lipases, CALB has a relatively short and rigid 'lid' region that partially covers the active site but does not exhibit the typical interfacial activation behavior, remaining catalytically active in homogeneous solutions. Recent studies have shown that structural modifications in the lid region directly influence the selectivity and efficiency of the enzyme. For example, specific mutations in the lid have shown potential to improve the selective acylation of amino acids such as lysine, highlighting the importance of this region in the interaction with chiral substrates.[6,7] Moreover, molecular dynamics analyses indicate that factors such as temperature, pH, and solvent can modulate the flexibility of the lid, impacting the accessibility of the active site and, consequently, enzymatic activity.[4-6]

The immobilization of enzymes on magnetic supports, especially on magnetic nanoparticles (MNs), has gained prominence in recent years due to the various advantages it offers for the development of reusable and highly stable biocatalysts. MNs are generally composed of iron oxides (such as $Fe_3O_4$) and can be functionalized with various chemical groups (e.g., amine, carboxyl, aldehyde) that enable stable binding with the enzyme. The advantages of immobilization on magnetic supports include easy magnetic separation, enabling rapid recovery of the enzyme after the reaction; reuse of the biocatalyst, which reduces operational costs; improved thermal and operational stability of the enzyme; and greater control over the orientation and immobilization density.[6,7] Moreover, magnetic nanoparticles exhibit the phenomenon of superparamagnetism (i.e., they do not retain magnetization after removal of the magnetic field), offering the advantage of a reduced risk of particle aggregation.[8] Another advantage is the high surface area that nanoparticles offer through a large surface-to-volume ratio, allowing for greater enzyme loading and facilitating the interaction between the enzyme and the substrate, which can enhance catalytic efficiency. Another positive aspect is the improvement in enzyme stability, since immobilization on nanoparticles can increase both the thermal and operational stability of enzymes, making them more resistant to variations in temperature and pH. However, depending on the production methodology, the main drawback is that the enzyme is exposed to the medium, and intermolecular processes may inactivate the enzyme. Another challenge in the use of magnetic nanoparticles is the high production costs associated with the synthesis and functionalization of nanoparticles, which can significantly impact the economic feasibility of large-scale applications. Furthermore, some nanomaterials may exhibit toxicity, which limits their use in food or pharmaceutical applications.[9] The magnetic nanoparticles are composed of biocompatible materials, such as magnetite, for use in bio-applications.[10] Thus, magnetic nanoparticles may efficiently support enzyme immobilization.[10-13] Remarkably, immobilized biocatalysts on magnetic nanoparticles can be easily recovered using a magnetic field, which may optimize operational costs and enhance product purity. The most common immobilization methods are: covalent binding using agents such as glutaraldehyde; physical adsorption, which is simpler but less stable; and magnetic cross-linked enzyme aggregates (mCLEAs), which combine enzyme precipitation and cross-linking on magnetic particles. These systems have been successfully applied in biodiesel synthesis, esterification/transesterification reactions, pharmaceutical and food processes, bioremediation, and wastewater treatment.[11-13]

Ibuprofen (2-(4-isobutylphenyl)propionic acid) is a crucial non-steroidal anti-inflammatory drug (NSAID), widely used in the treatment of conditions such as cephalgia, headache, muscular strain, and rheumatoid arthritis.[14,15] As with most profens, ibuprofen has a stereogenic center and is marketed as a racemic carboxylic acid, in which the (*S*)-enantiomer is responsible for the target therapeutic effect and is approximately 160 times more active than the (*R*)-enantiomer in the *in vitro* inhibition of prostaglandin biosynthesis.[16] Besides being considered inactive, (*R*)-ibuprofen is inappropriate due to its side effects on the gastrointestinal tract, membrane function, and normal lipid metabolism.[14-17] Furthermore, other advantages can be reached with the administration of pure (*S*)-enantiomers, such as reduced metabolic load and pharmacokinetic interactions with other drugs.[18] Thus, the use (*S*)-enantiomer is preferable rather than the racemic mixture.[16] The enzymatic resolution of ibuprofen has been considered preferable instead of classical methods, as chromatographic separation and enantioselective crystallization can be performed by several lipases.[19] To decrease the side effects, the development of prodrugs for NSAIDs has been searched for the blockage of the carboxylic acid group of NSAIDs.[13] Using esterification

for the kinetic resolution of proteins is an exciting method for prodrug preparation.[16]

This work evaluated the immobilization of CALB on activated magnetic iron nanoparticles. The biocatalysts produced were characterized using different techniques, including X-ray powder diffraction (XRD) and Fourier transform infrared (FTIR) spectroscopy, which confirmed the incorporation of magnetite and the immobilization of CALB within the magnetite matrix. The influence of operational conditions, such as stirring speed, enzyme load, contact time, and the presence of additives during immobilization, substances that can enhance or inhibit immobilization, such as glutaraldehyde, which is used to form covalent bonds between the enzyme and the support or between enzyme molecules, increasing stability, was addressed.[13,14] The resulting biocatalyst was tested in the esterification of racemic ibuprofen. The results obtained with MNs-CALB (lipase B from *Candida antarctica* immobilized on magnetite functionalized in γ-aminopropyltriethoxysilane (APTS) and activated with glutaraldehyde) were compared to those obtained for CALB immobilized on the acrylic resin (Novozym® 435 - Commercial CALB). Furthermore, molecular docking studies were conducted to elucidate the esterification reaction between ibuprofen and CALB.[13,15,16]

Regarding the advantages and disadvantages of this study, although the use of toxic organic solvents is common in esterification reactions, it can be seen as an environmental limitation. Greener studies that use aqueous systems or sustainable solvents currently have an advantage. A relevant application of this work is the chiral resolution of (*R*,*S*)-ibuprofen, a significant pharmaceutical application. Articles dealing with real and industrial applications of this kind attract greater interest. The study of operational parameters, including agitation speed, enzyme loading, contact time, glutaraldehyde concentration, and the presence of additives, demonstrates a systematic and comprehensive approach - this type of analysis is highly valued, especially when optimization is sought. Computational analysis (molecular docking), such as the inclusion of docking studies to investigate interactions with the catalytic triad, shows a multidisciplinary effort, which increases the impact and scope of the work.[15,19]

## Experimental

### Materials and reagents

The chemical reagents used in this study include $FeCl_3.6H_2O$ (pure granulated 99%), $FeSO_4.7H_2O$ (pure granulated 99%), and 30% ammonia solution. Lipase B from *Candida antartica* (CALB) was purchased from Codexis (Redwood, USA). Lipase B from *Candida antartica* immobilized on the acrylic resin (Novozym® 435), aminopropyltriethoxysilane (APTS), glutaraldehyde solution grade II 25% (m/v), *p*-nitrophenyl butyrate (*p*-NPB), and *p*-nitrophenol (*p*-NP) were purchased from Sigma-Aldrich (St. Louis, USA). All other reagents (analytical grade) were purchased from Synth (São Paulo, Brazil) and Vetec (São Paulo, Brazil).

### Methods

#### Synthesis of $Fe_3O_4$ magnetic nanoparticles

The coprecipitation method produces magnetic iron nanoparticles ($Fe_3O_4$) with an approximate particle size of 11.0 nm.[20] A solution of metal salts containing $Fe^{2+}$ and $Fe^{3+}$ ($FeSO_4 7H_2O$ and $FeCl_3 6H_2O$, 1:2) was mixed and diluted in Milli-Q water to form the spinel phase ($Fe_3O_4$). The aqueous mixture was heated to 70 °C under constant stirring, and a 30 wt.% $NH_4OH$ solution (ammonium hydroxide) was added until the pH reached 10, resulting in the formation of a black precipitate. The residue was washed several times with Milli-Q water until the residual solution reached neutral pH, followed by a final single rinse with methanol. The sample of MNs was then dried in a desiccator under vacuum.

#### Surface modification and activation of MNs (magnetic nanoparticles - magnetite - $Fe_3O_4$)

Iron magnetic nanoparticles were modified with aminopropyltriethoxysilane (APTS). The reaction was initiated by adding a solution of 2.0% v/v APTS to the support suspension. The solution was heated at 100 °C for 10 h under a nitrogen atmosphere. The modified nanoparticles were washed with 100 mL of methanol and 100 mL of ethanol, separated by magnetic decantation, and dried at 30 °C for 24 h.[11]

#### Glutaraldehyde activation

Iron magnetic nanoparticles modified with aminopropyltriethoxysilane (10 mg) were suspended in a glutaraldehyde solution (2.5 or 25% m/v) with a 2.5 ratio solution/support (mL $g^{-1}$). The mixture was stirred (20-250 rpm) for two hours at 25 °C. Finally, supports were washed with a 100 mM bicarbonate buffer, pH 10, to remove the excess of activating agent.[10]

#### Lipase B from *Candida antartica* - CALB immobilization

Immobilization of CALB on the previously activated support was carried out in batch mode at 25 °C. 0.5 mL of the enzyme (0.16-0.51 mg) in sodium bicarbonate

buffer (100 mM, pH = 10) was added to 0.01 g ($Fe_3O_4$). The stirring speed was over the range of 20 to 250 rpm. Two types of stirring were studied: rotational (20-45 rpm) and orbital (20-250 rpm). Contact time was also evaluated, ranging from 0.5 to 5 h. Last, the influence of additives (sodium dodecyl sulfate 0.23%, SDS) during immobilization was verified. The immobilized CALB, designated as MNs-CALB, was removed by magnetic separation and washed with a sodium bicarbonate buffer (100 mM, pH 10.0). The amount of CALB immobilized on magnetic nanoparticles (MNs) was determined by measuring the initial and final concentration of CALB in the immobilization supernatant. The hydrolytic activity assay was used to calculate key immobilization parameters: immobilization yield (IY), theoretical activity (Att), and recovery activity (Atr).[21]

### Characterization of the supports and biocatalysts

#### Vibrating sample magnetometer (VSM) analysis: magnetic study

Magnetic curves were generated using a vibrating sample magnetometer (VSM) at 300 K. To ensure the accuracy of the acquired magnetic moments, the VSM underwent prior calibration with standard reference materials. In all measurements, the magnetic moment obtained for each applied field was normalized by the mass of the nanoparticles.

#### Scanning electron microscopy (SEM) coupled with X-ray fluorescence (XRF) spectroscopy

Morphology and chemical composition were assessed by scanning electron microscopy (SEM) imaging coupled with energy-dispersive X-ray spectroscopy (EDS) using the QUANTA 450 FEG microscope. Magnetic measurements were performed by vibrating sample magnetometry (VSM). The samples were affixed to carbon tape and silver-coated using the Quorum QT150ES metallization equipment, followed by a 20 kV electron beam. XRF analysis was performed using a Shimadzu model EDX-7000 instrument equipped with a rhodium tube, with 4 kV of power applied to the powdered samples.

#### Fourier transform infrared spectroscopy (FTIR)

Fourier transform infrared (FTIR) spectra were obtained using a PerkinElmer 2000 spectrophotometer, spanning a wavenumber range from 4000 to 400 $cm^{-1}$. Before analysis, the samples were pre-dried to eliminate water absorption and dispersed in KBr at a 1:10 ratio. Subsequently, they were fashioned into translucent tablets with the assistance of a hydraulic press.

### Enzyme assay and protein determination

#### Determination of enzyme activity

The activity of MNs-CALB (lipase B from *Candida antarctica* immobilized on magnetite functionalized in APTS and activated with glutaraldehyde) was determined spectrophotometrically using 50 mmol $L^{-1}$ *p*-nitrophenyl butyrate (*p*-NPB) in acetonitrile. The reaction mixture was prepared by mixing 50 µL of *p*-NPB with 2.5 mL of 25 mmol $L^{-1}$ sodium phosphate buffer at pH 7, and then adding either 50 µL of the sample or 10 mg of biocatalyst at 25 °C. The product released during the hydrolysis of *p*-NPB, *p*-nitrophenol, was quantified by spectrometry using a spectrophotometer (Thermo Scientific®) at a wavelength of 348 nm ($\varepsilon$ = 10.052 $M^{-1}$ $cm^{-1}$). One unit of activity (U) was defined as the amount of enzyme that hydrolyzes 1 µmol of substrate (*p*-NPB) *per* min under the conditions cited above.[22] The protein concentration was determined by the Bradford method, and bovine serum albumin was used as standard.[23]

#### Thermal stabilities of soluble and immobilized CALB

The thermal stability of both soluble and immobilized CALB at 60 °C was evaluated by measuring the residual activity through the hydrolysis of *p*-nitrophenyl butyrate (*p*-NPB). Soluble or immobilized CALB was incubated in 25 mM sodium phosphate buffer, pH 7, at 60 °C, for 48 h. Samples were periodically withdrawn, and their residual activities were assayed. The deactivation constant and half-life ($t_{1/2}$) were calculated according to Sadana and Henley's model.[24] Stabilization factors were obtained as the ratio between half-lives of the immobilized and the soluble CALB.[21]

#### Operational stability of the immobilized CALB

The operational stability of hydrolysis of the immobilized lipase was determined by six subsequent cycles of hydrolysis reactions of *p*-NPB. After each cycle, the nanoparticles were separated using a magnetic field, washed with 25 mM sodium phosphate buffer (pH 7), and recycled.

### Application of the biocatalyst in the esterification model reaction

#### Racemic ibuprofen esterification

The reaction medium comprised cyclohexane, racemic ibuprofen, and 1-propanol. The reaction was started by adding immobilized CALB into the reaction medium. The suspension was incubated at 37 °C and shaken at 600 rpm in a thermomixer for 24 to 72 h. Samples (50 µL)

were periodically withdrawn throughout the incubation period. The collected supernatant was evaporated at room temperature, and the residue was dissolved in 0.7 mL of mobile phase for HPLC (high-performance liquid chromatography) analysis.[16]

### Study *in silico*

#### Preparation of binders and proteins

The molecules of (*R*)-(−)-ibuprofen and (*S*)-(+)-ibuprofen were created using Chem3D software,[25] as shown in Figure 1, employing the auto-optimization settings with the MMFF94S force field.[26]

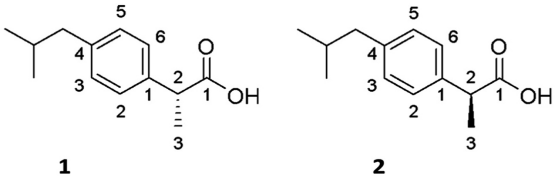


**Figure 1.** 2D molecular structures of (*R*)-(−)-ibuprofen (**1**) and (*S*)-(+)-ibuprofen (**2**).

This process aimed to generate bioactive conformations through the minimization of randomly generated conformers, using the Steepest Descent algorithm,[27] and Step *per* Update 4,[28] facilitated by Avogadro software.[29] All files with ligands were converted to corresponding formats (pdbqt) with the addition of ionization and tautomeric states at pH 7.4 by using OpenBabel version 3.0.0 software.[30]

The receptor under study was the structure of the lipase CALB, obtained from the Protein Data Bank repository (code 1TCA),[31] whose crystalline structure was determined by complex X-ray diffraction. The interfering residues, water molecules, and the synthetic inhibitor were removed from the structure. Furthermore, polar hydrogens were added to both the ligands and the protein. The software used was Autodock Tools.[32]

#### Molecular docking

Molecular docking was performed using AutoDock Vina,[33,34] employing three-way multithreading. For docking of CALB lipase (1TCA), the following parameters were used: number of grid points in xyz dimensions (30, 30, 30), grid spacing (0.642 Å), grid center coordinates in xyz (-2.847793, 22.862241, 14.848931). All other parameters were set to default values. The input ligands, which included polar hydrogens, were prepared in the pdbqt format. Between ten and forty molecular docking executions were conducted, with multiple simulations repeated in the same region of the biological receptor. Thus, to validate the performance of the simulations and assess the quality of the docking study, the RMSD (root mean square deviation) scoring criterion was adopted, indicating that a successful docking should exhibit a RMSD ≤ 2.0 Å.[35]

The simulation data, including the main receptor-ligand interactions, were visualized using the Discovery Studio software.[36]

## Results and Discussion

#### Effect of different glutaraldehyde concentrations on CALB immobilization

To facilitate covalent bonding between the enzyme and the support, glutaraldehyde was employed as a cross-linking agent due to its effectiveness in forming stable covalent bonds with amine groups on the enzyme surface. The CALB enzyme contains free amino groups (such as those present in the lysine residues of its structure). When incubated with a glutaraldehyde-activated support, CALB covalently binds to the surface through a reaction between the aldehyde group of the glutaraldehyde already attached to the support and the amino groups of the enzyme. This interaction forms a stable and insoluble network, effectively anchoring the enzyme to the support.[37]

When glutaraldehyde is used in enzyme immobilization processes, such as in the case of CALB (*Candida antarctica* lipase B), it is essential to ensure that it does not cause residual toxic effects in the final product. Glutaraldehyde is highly reactive and can be harmful if not adequately controlled. In this study, several procedures were employed to minimize potential glutaraldehyde toxicity, supported by evidence from the literature. These included the quantification of residual glutaraldehyde after the immobilization process. At this stage, the enzymatic support was thoroughly washed with an appropriate buffer, in the case of CALB, a 100 mM bicarbonate buffer at pH 10.[38]

Another precautionary measure was the inclusion of a control, consisting of the support treated with glutaraldehyde but without the enzyme, to confirm that any observed activity was indeed due to the enzyme and not due to interference from the toxic agent. This study was conducted under the optimal conditions reported in previous research,[22] which employed similar glutaraldehyde concentrations and reaction times and did not observe residual toxicity, thereby further strengthening the foundation of this work.

Figure 2 shows CALB activity during immobilization without the use of glutaraldehyde (0%), the influence of different glutaraldehyde concentrations (2.5 or 25%), and

the effect of an additive (0.23% SDS) on the activity of the derivative. A strong correlation was observed between the immobilized enzyme activity and glutaraldehyde concentration, with activity increasing approximately 13-fold at 25% concentration. The exact amount of enzyme was measured at each stage, i.e., the enzymatic activity before immobilization, which was 0.546 U $mL^{-1}$.

The enhancement observed at higher glutaraldehyde concentration indicates the formation of a denser and more stable enzyme-support matrix, resulting in improved conformational rigidity and reduced desorption during catalysis. This effect has also been reported by other authors, who demonstrated that stronger multipoint covalent attachment increases enzyme robustness and preserves catalytic activity under mechanical or thermal stress.[39-41] However, excessive cross-linking may lead to partial modification of catalytically essential residues or to over-rigidification of the enzyme structure, potentially decreasing flexibility in the active site. Therefore, achieving an optimal balance of glutaraldehyde concentration is critical to ensure both stability and activity.

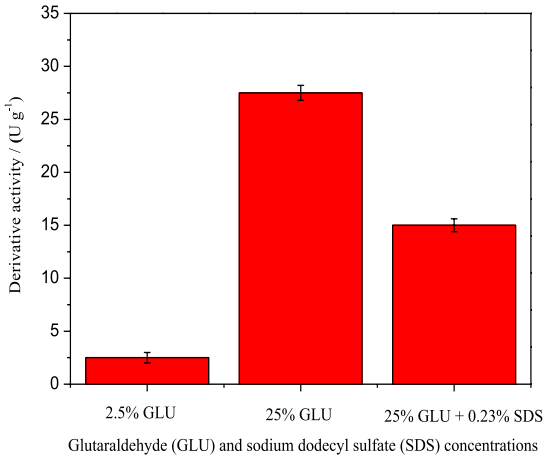


**Figure 2.** Effect of additives sodium dodecyl sulfate (SDS) and glutaraldehyde (GLU) concentration on immobilization of lipase B from *Candida antarctica* (CALB) in magnetic nanoparticles (MNs). (■) Derivative activity.

Generally, the specific surface area of smaller particles, such as nanoparticles, is significantly higher than that of larger particles, resulting in a greater density of reactive sites *per* unit mass. Consequently, a larger surface area demands higher concentrations of glutaraldehyde to ensure sufficient coverage and effective cross-linking of all available amine groups on the support surface. In this context, different authors have reported that high glutaraldehyde concentrations are essential to achieve extensive activation of the carrier and to form stable covalent linkages with enzyme molecules.[10,39,40] Such concentrations are crucial to promote multipoint attachment, increasing the number of enzyme-carrier interactions and creating a more rigid enzyme microenvironment that enhances both the mechanical robustness and the intrinsic activity of the immobilized enzyme.[41]

At the molecular level, glutaraldehyde reacts with primary amino groups, forming Schiff bases or imine bonds that effectively "lock" flexible regions of the protein to the functionalized nanoparticle surface. This network reduces the conformational entropy of the enzyme, thereby stabilizing the tertiary structure against unfolding or desorption during catalytic turnover. However, this same rigidity can introduce a trade-off: if the cross-linking density becomes excessive, it can restrict subtle but essential motions in regions surrounding the catalytic triad or hinder substrate diffusion into the active site. Consequently, while higher glutaraldehyde concentrations (such as 25%) enhance stability, over-rigidification may cause partial loss of activity due to steric hindrance or modification of catalytically essential residues, such as Lys, Ser, or His side chains involved in the microenvironment of the active site.[40,41] Therefore, optimizing the glutaraldehyde concentration is a critical design step, as it governs the delicate balance between enzyme rigidity (for stability) and flexibility (for activity).

The influence of additives such as surfactants during immobilization has also been extensively explored in lipase systems, where these molecules can induce interfacial activation. In principle, surfactants adsorb at hydrophobic regions of the enzyme, shifting it from the "closed" to the "open" conformation, thereby exposing the catalytic site and enhancing accessibility to substrates. Cross-linking in the presence of such additives can, in theory, stabilize the enzyme in this open form, improving catalytic efficiency and selectivity. Moreover, because surfactants are not covalently attached, they can be easily removed after immobilization, leaving behind a conformation that is more catalytically competent.[42]

In this study, the anionic surfactant SDS was evaluated for its effect on CALB immobilization parameters. SDS has been reported to enhance the catalytic activity of many lipases by maintaining an open-lid conformation and increasing interfacial contact with hydrophobic substrates.[43,44] However, as shown in Figure 2, the inclusion of SDS (0.23%) did not improve the performance of CALB; on the contrary, the resulting derivative exhibited only 15.8 U $g^{-1}$ of activity, nearly half the value observed in the absence of the surfactant (29.1 U $g^{-1}$). This inverse effect can be rationalized by the structural features of CALB itself: unlike most lipases, CALB possesses a relatively small and rigid lid region and lacks pronounced interfacial

activation behavior.[45] Thus, SDS does not confer the same conformational benefit as seen in classical interfacially activated lipases (e.g., from *Thermomyces lanuginosus* or *Rhizomucor miehei*), and may instead disturb essential intramolecular hydrogen bonds or the microenvironment surrounding the catalytic Ser[105].

Furthermore, the concentration of SDS used (0.23%) approaches levels known to perturb protein tertiary structure. As an anionic detergent, SDS interacts with hydrophobic regions of the enzyme, disrupting noncovalent interactions such as hydrophobic packing and hydrogen bonding, leading to partial unfolding or even denaturation. This destabilization likely compromised the native conformation of CALB, explaining the observed decrease in activity. In addition, SDS may have interfered with the immobilization matrix or with the glutaraldehyde activation chemistry itself by competing for surface adsorption sites or by masking amine groups, thereby reducing the formation of productive enzyme-support covalent bonds. Hence, SDS, at this concentration, hinders rather than enhances immobilization efficiency.[44,45]

Taken together, these results indicate that although surfactant-assisted immobilization can be beneficial for lipases exhibiting strong interfacial activation, such as lipase A from *Candida rugosa* or lipase from *Thermomyces lanuginosus*, it is not suitable for CALB. In fact, for enzymes with smaller or less flexible lid regions, maintaining the natural conformation without surfactant exposure is a more effective strategy. Therefore, the use of SDS in enzyme immobilization protocols should be carefully controlled and limited to concentrations well below those typically used for protein denaturation.

Finally, the operational stability of MNs-CALB derivatives (lipase B from *Candida antarctica* immobilized on magnetite functionalized with APTS and activated with glutaraldehyde), obtained under different additive and cross-linking conditions, was investigated through consecutive hydrolysis cycles, as shown in Figure 3. The comparative performance of these derivatives provided further insights into how molecular - level interactions established during immobilization translate into macroscopic catalytic durability - a crucial property for industrial reuse and process economy.

The results clearly demonstrate that the biocatalyst immobilized in the absence of surfactant exhibited superior operational stability compared to the system prepared with SDS. In particular, the MNs-CALB derivative synthesized without any additive maintained more than 50% of its initial catalytic activity after five consecutive hydrolysis cycles, confirming that the covalent anchoring between CALB and the APTS/GLU-modified magnetic nanoparticles produced

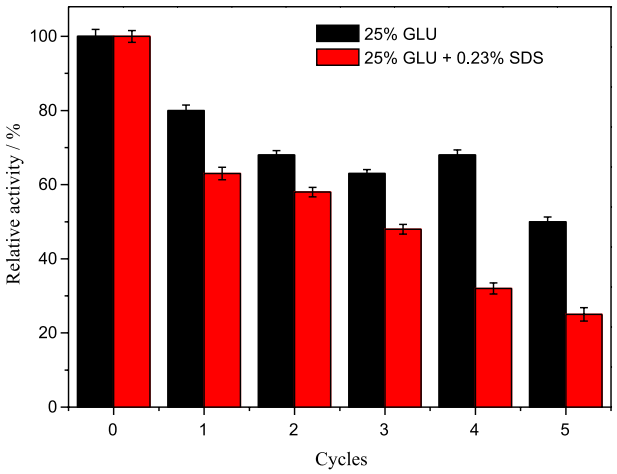


**Figure 3.** Operational stability in the hydrolysis of *p*-nitrophenyl (*p*-NPB) butyrate to lipase B from *Candida antarctica* immobilized on magnetite functionalized in APTS and activated with glutaraldehyde (MNs-CALB). Additives: 25% glutaraldehyde (black bars) and (25% glutaraldehyde + 0.23% SDS) (red bars).

a robust and reusable system. Conversely, the derivative obtained in the presence of SDS retained less than 30% of its original activity under identical conditions, indicating partial enzyme deactivation or desorption from the carrier during repeated use.

This contrast reinforces the mechanistic interpretation that the detergent introduced structural perturbations in the enzyme or interfered with the covalent attachment process, generating a less stable catalytic network. Moreover, the absence of surfactant favored a more homogeneous distribution of CALB molecules over the nanoparticle surface and a more compact cross-linked configuration, minimizing conformational stress during successive catalytic cycles. Thus, the system prepared without SDS not only achieved higher immobilization efficiency but also provided enhanced structural resilience and better preservation of the active conformation throughout repeated operational use.

## Biophysical characterization of magnetic nanoparticles (MNs) and MNs-CALB derivatives

### Magnetic study of the synthesized supports

The magnetic behavior of the synthesized nanomaterials was evaluated through VSM, and the magnetization curves are presented in Figure 4. The results reveal that the pristine magnetic nanoparticles (MNs) exhibited a saturation magnetization ($M_s$) of approximately 73 emu $g^{-1}$, while the sequential surface modifications led to a gradual decrease: 67 emu $g^{-1}$ for MNs/APTS (γ-aminopropyltriethoxysilane-functionalized particles), 50 emu $g^{-1}$ for MNs/APTS/GLU (after activation with glutaraldehyde), and 42 emu $g^{-1}$ for MNs-CALB (the final biocatalyst containing immobilized *Candida antarctica* lipase B).

This progressive reduction in magnetization is consistent with literature reports, which attribute such behavior to the introduction of non-magnetic organic layers onto the magnetite surface.[46] Each functionalization step-first with APTS silanization, then with glutaraldehyde cross-linking, and finally with enzyme coating-incrementally increases the proportion of organic matter surrounding the magnetic core, thereby diluting its overall magnetic moment. Importantly, even after complete biocatalyst formation, the MNs-CALB derivative maintained a substantial magnetic response, sufficient to enable rapid and efficient recovery by a low-intensity external magnetic field.

The preservation of magnetic responsiveness after immobilization is a key feature for industrial applications, as it allows for catalyst separation and reuse without the need for filtration or centrifugation steps. Furthermore, the decrease in saturation magnetization (Ms) observed here also indirectly confirms the successful formation of the multilayer organic shell, supporting the FTIR and SEM analyses that demonstrate effective functionalization. In practical terms, this combination of strong magnetic response and controlled surface modification ensures that the synthesized MNs-CALB biocatalyst possesses both physicochemical stability and operational manageability-two essential attributes for its deployment in scalable bioprocesses involving repeated catalytic cycles.

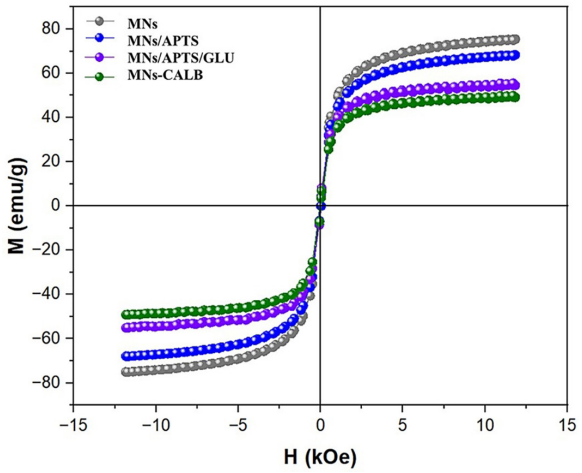


**Figure 4.** Magnetic characterization of synthesized materials and biocatalysts: MNs - magnetic nanoparticles (magnetite - $Fe_3O_4$); MNs/APTS (MNs functionalized with γ-aminopropyltriethoxysilane); MNs/APTS/GLU (MNs functionalized with APTS and activated with glutaraldehyde; MNs-CALB: lipase B from *Candida antarctica* immobilized on magnetite functionalized in APTS and activated with glutaraldehyde.

The gradual reduction in the $M_s$ observed after each functionalization step - from bare MNs to MNs/APTS, MNs/APTS/GLU, and finally MNs-CALB - reflects the progressive incorporation of non-magnetic organic layers onto the magnetic core. This attenuation of $M_s$ after silanization with APTS and subsequent activation with glutaraldehyde is fully aligned with what has been reported for $Fe_3O_4$-based nanosystems functionalized for biocatalytic purposes,[46] where surface coating with organosilane linkers and cross-linking agents inevitably dilutes the net magnetic moment *per* gram of material. In practical terms, each new chemical layer deposited on the nanoparticle surface increases the mass fraction of diamagnetic or weakly paramagnetic species (silanes, aldehyde linkers, adsorbed enzyme), but does not contribute to magnetization. As a result, even though the magnetic core (magnetite) retains its intrinsic ferrimagnetic behavior, the normalized $M_s$ value measured *per* gram of total material decreases.

This reduction in $M_s$ is not indicative of a loss of magnetic integrity or structural degradation of the $Fe_3O_4$ core. Instead, it is an expected physical consequence of building a hybrid organic-inorganic architecture in which biological functionality is added at the expense of pure magnetic mass. Importantly, despite this decrease, the final MNs-CALB derivative still exhibited a sufficiently high magnetization (ca. 42 emu $g^{-1}$) to allow fast and efficient magnetic recovery. In other words, even after sequential surface modification with APTS, subsequent activation with glutaraldehyde, and covalent immobilization of CALB, the particles remained strongly responsive to an external magnetic field and could be rapidly separated from the reaction medium without the need for centrifugation or filtration. This is a crucial operational attribute for industrial biocatalysis, since it minimizes downstream processing costs and enables straightforward catalyst recycling in batch or semi-continuous systems.

From an application standpoint, the fact that the $M_s$ values decrease but do not collapse confirms two things: (*i*) the functionalization chemistry was successful - because the organic coating is directly responsible for the observed drop in magnetization - and (*ii*) the structural core of magnetite remains intact and magnetically competent. Thus, the immobilization strategy preserved the essential benefit of magnetic nanocarriers (i.e., recoverability under low-intensity magnetic fields) while simultaneously introducing biochemical functionality (enzyme anchoring, stabilization, reusability). Taken together, the VSM results indicate that neither silanization nor cross-linking nor enzyme loading compromised the practical manipulability of the nanosystem. Instead, they resulted in a robust magnetically recoverable biocatalyst with controlled surface chemistry, which is precisely the desired profile for recyclable enzymatic systems targeted to fine-chemical and pharmaceutical applications, where catalyst retention and product purity are critical.

### Scanning electron microscopy (SEM) and X-ray fluorescence (XRF)

The morphological and compositional evolution of the supports throughout the different functionalization steps was further examined by SEM and XRF (Figures 5a-5d and insets). The SEM micrographs reveal clear differences between the pristine MNs and the progressively modified systems (MNs/APTS, MNs/APTS/GLU, and MNs-CALB), indicating that each surface treatment step leaves a detectable imprint on particle organization, texture, and apparent agglomeration state. The initial MNs display the typical granular/micrometric aggregates that arise from the clustering of primary $Fe_3O_4$ nanoparticles, suggesting high surface roughness and a heterogeneous porosity that is favorable for enzyme anchoring. After APTS functionalization (MNs/APTS), the surface appears more uniformly coated, consistent with silane deposition over the magnetic core. This tends to smooth local asperities and can partially bridge adjacent particles, promoting the formation of denser agglomerates stabilized by the organosilane network.

Following activation with glutaraldehyde (MNs/APTS/GLU), additional changes in surface texture are observed, compatible with the introduction of a cross-linked organic layer. This activated interface provides aldehyde groups that subsequently react with nucleophilic residues of CALB. In the final biocatalyst (MNs-CALB), the SEM images suggest the presence of an additional organic corona associated with the immobilized lipase layer. This organic coverage can act as a physical "skin" over the nanoparticle clusters, which not only stabilizes the enzyme at the solid-liquid interface but also helps prevent extensive nanoparticle coalescence. Such a morphology is consistent with a system in which the enzyme is not merely adsorbed but covalently anchored, forming a cohesive bioinorganic shell rather than isolated protein patches.

The XRF elemental maps (insets in Figure 5) complement the SEM observations by confirming the predominance of iron (Fe) in all samples, as expected for magnetite-based carriers, while also revealing progressive incorporation of other elements associated with surface chemistry and bioconjugation. The slight relative decrease in Fe signal intensity and the increasing contributions of light elements and sulfur ("others" and S in the provided maps) across MNs → MNs/APTS → MNs/APTS/GLU → MNs-CALB are consistent with stepwise addition of organic functional groups and biomolecules. This chemical signature supports the interpretation that (*i*) silanization effectively grafted APTS to the nanoparticle surface, (*ii*) glutaraldehyde activation introduced further non-magnetic organic content, and (*iii*) CALB immobilization successfully anchored the enzyme layer onto the functionalized support.

Altogether, the SEM and XRF results show that the immobilization route did not simply decorate the surface in a superficial, weakly adsorbed way. Instead, the data indicate the formation of an integrated hybrid structure in which the inorganic core (magnetite) provides mechanical and magnetic support, while the organic shell (APTS/GLU + CALB) defines the catalytic interface. This hierarchical organization is crucial for performance: the nanoparticle core guarantees rapid magnetic recovery and processability, whereas the chemically tailored outer layer creates a biocompatible microenvironment for the lipase, helping preserve activity, orientation, and accessibility to substrates during catalysis and reuse.

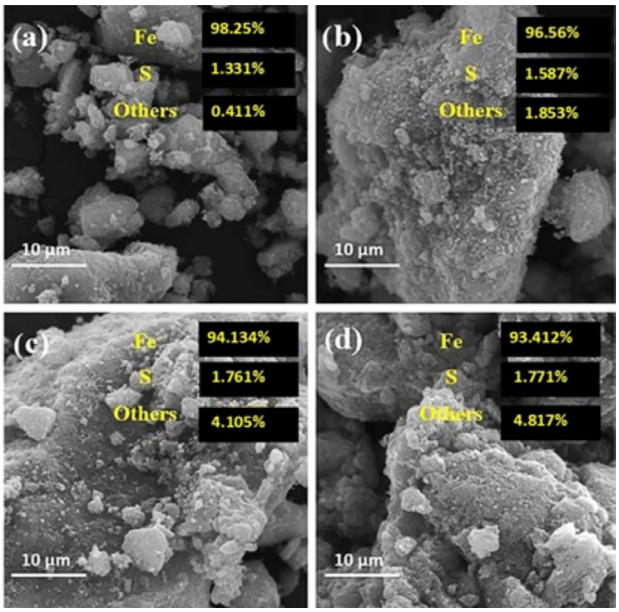


**Figure 5.** VSM and XRF images of: (a) MNs - magnetic nanoparticles; (b) MNs/APTS - magnetite functionalized with APTS (γ-aminopropyltriethoxysilane); (c) MNs/APTS/GLU - magnetite functionalized with APTS and activated with GLU (glutaraldehyde); (d) MNs-CALB: lipase B from *Candida antarctica* immobilized on magnetite functionalized with APTS and activated with glutaraldehyde.

The XRF elemental maps confirmed that all samples exhibited surfaces homogeneously enriched with iron, validating the successful synthesis of magnetite nanoparticles. The dominance of Fe peaks across all formulations reflects the preservation of the crystalline $Fe_3O_4$ phase even after multiple functionalization steps. Slight but consistent reductions in Fe intensity were observed for the APTS- and GLU-modified systems, accompanied by the progressive appearance of secondary elements such as sulfur and other light atoms. These variations are a clear indication of successive chemical

modifications on the nanoparticle surface, with the incorporation of organic functional groups and enzyme molecules contributing to the overall compositional heterogeneity of the hybrid system.

In particular, the emergence of sulfur and carbon-rich signals after APTS and glutaraldehyde treatments demonstrates that the nanoparticle surfaces became progressively coated with non-magnetic, organic material-consistent with the formation of a cross-linked silane-aldehyde network that provides anchoring sites for CALB. The presence of iron at the outermost surface of the final MNs-CALB sample (Figure 5d) further confirms that, despite the organic coverage, the magnetic core remains partially exposed, enabling effective magnetic responsiveness. This balance between organic functionalization and magnetic accessibility is desirable for biocatalytic applications, as it ensures both biochemical compatibility and facile magnetic recovery of the biocatalyst from reaction media.

### Fourier transform infrared spectroscopy (FTIR) analysis

The structural and chemical evolution of the materials was further examined by FTIR spectroscopy (Figure 6). All systems exhibited characteristic absorption bands between 567 and 625 $cm^{-1}$, attributed to Fe–O stretching vibrations of magnetite.[46,47] The persistence of these bands across all samples demonstrates that the crystalline integrity of the $Fe_3O_4$ core was preserved during each functionalization stage. Additionally, broad absorption at 3427 $cm^{-1}$ and a weaker band around 1627 $cm^{-1}$ were consistently observed in all spectra, corresponding to the stretching and bending vibrations of hydroxyl (–OH) groups and adsorbed water molecules on the nanoparticle surface.[47,48] These surface hydroxyl groups play a central role in subsequent silanization, serving as anchoring points for APTS molecules.

In the MNs/APTS spectrum (Figure 6b), the appearance of a distinct band at 1126 $cm^{-1}$ is diagnostic of Si–O–Fe bonding, confirming the successful grafting of aminopropylsilane chains onto the magnetite surface.[49] This covalent linkage provides terminal amine groups that enable further activation with bifunctional cross-linkers such as glutaraldehyde. Following this step, the MNs/APTS/GLU spectrum (Figure 6c) displayed a new absorption peak at 1742 $cm^{-1}$, corresponding to the C=O stretching vibration of aldehyde groups, providing direct evidence of successful glutaraldehyde coupling to the silanized surface.[50] Importantly, the Fe–O band of magnetite remained unaltered, indicating that the activation reaction was confined to the outer functional layer and did not perturb the magnetic core.

After enzyme immobilization, the MNs-CALB spectrum revealed additional bands near 1437 $cm^{-1}$, which can be assigned to N–H bending and C–N stretching vibrations associated with peptide linkages from the protein backbone.[49] The presence of these amide-related bands confirms the covalent attachment of CALB molecules to the glutaraldehyde-activated surface through Schiff-base formation between aldehyde and lysine residues. The combination of these vibrational features-Si–O–Fe, C=O (aldehyde), and amide bands-constructs a consistent chemical narrative of sequential surface modification: silanization, activation, and enzyme immobilization.

Overall, the FTIR results substantiate the formation of a well-organized hierarchical architecture in which the magnetite core provides magnetic functionality, the APTS-GLU network offers reactive anchoring sites, and the outer CALB layer supplies catalytic activity. This multilayered configuration is critical for generating a biocatalyst that unites structural stability, high enzyme loading, and magnetic separability, fulfilling the design principles for advanced recyclable nanosystems.

The mechanical environment during immobilization plays a decisive role in determining enzyme-support interactions, diffusion phenomena, and the final conformational state of the immobilized biocatalyst. Stirring, in particular, governs the hydrodynamic shear forces acting on enzyme molecules in suspension. At moderate agitation levels, the shear rate promotes efficient dispersion of the nanoparticles and enhances the probability of enzyme-support collisions, facilitating covalent bond formation and uniform coating of the carrier surface. Under such conditions, mixing reduces diffusional limitations and ensures better accessibility of functional groups, thereby favoring high immobilization yields and catalytic activity.

However, when the shear rate exceeds a critical threshold, the benefits of agitation are counteracted by mechanical stress imposed on the enzyme molecules. High shear intensity can lead to partial unfolding of the protein structure, particularly at the interfacial region where the lipase interacts with gas-liquid or solid-liquid boundaries. Such conditions promote transient exposure of hydrophobic regions, aggregation, or even irreversible denaturation. Furthermore, excessive turbulence may generate microbubbles that enhance interfacial stress, accelerating conformational fatigue and inactivation of the biocatalyst. These effects are especially critical for lipases, whose catalytic performance is closely linked to the integrity and flexibility of their active-site lid domain.[51]

Interestingly, immobilization on nonporous supports such as APTS/GLU-functionalized magnetite does

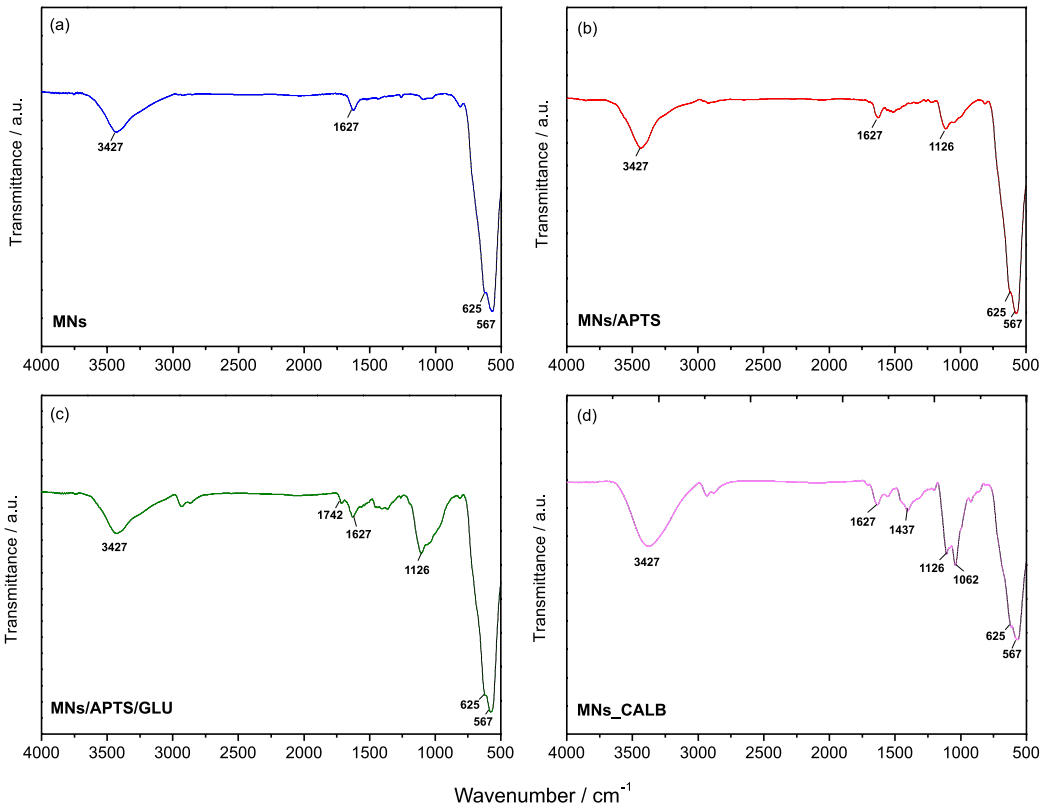


**Figure 6.** FTIR spectra of the samples recorded in the 4000-400 $cm^{-1}$ range using the KBr pellet method: (a) MNs - magnetic nanoparticles; (b) MNs/APTS - magnetite functionalized with APTS (γ-aminopropyltriethoxysilane); (c) MNs/APTS/GLU - magnetite functionalized with APTS and activated with GLU (glutaraldehyde); (d) MNs-CALB: lipase B from *Candida antarctica* immobilized on magnetite functionalized with APTS and activated with glutaraldehyde. Effect of the stirring speed on the immobilization of CALB onto MNs.

not fully mitigate shear-induced inactivation, since the immobilization interface is external and directly exposed to hydrodynamic forces. In porous matrices, the enzyme can be physically shielded within confined environments, but in the present system, the absence of protective microcavities leaves the immobilized CALB more susceptible to surface shear. This highlights the need to carefully control the agitation regime during immobilization to balance efficient mixing with structural preservation of the enzyme.

Therefore, to optimize process conditions for the CALB system, the effect of stirring speed on enzyme immobilization was systematically investigated, as shown in Figure 7. By evaluating immobilization efficiency, recovered activity, and potential conformational damage across a range of agitation intensities, it was possible to establish an operational window in which mass transfer is maximized without inducing significant mechanical deactivation. Such an approach provides valuable insight for scaling up the immobilization process, where reactor geometry and fluid dynamics can drastically influence enzyme stability and overall biocatalyst performance.

The influence of stirring mode-orbital *versus* rotational was systematically evaluated to understand how hydrodynamic conditions affect enzyme attachment and

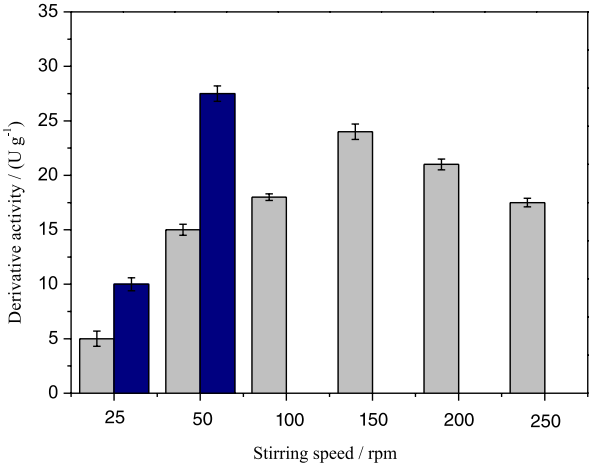


**Figure 7.** Effect of stirring speed during the immobilization process on the resulting MN-CALB derivatives (lipase B from *Candida antarctica* immobilized on magnetite functionalized in APTS and activated with glutaraldehyde). Activities are displayed for derivatives obtained through rotational stirring (dark blue bars, 25-50 rpm) and orbital stirring (light gray bars, 25-250 rpm).

activity recovery. Due to equipment constraints, rotational stirring could be examined only at 20 and 45 rpm, whereas orbital stirring was explored across a wider range, from 20 to 250 rpm, with a fixed immobilization time of one hour for all conditions.

A pronounced dependence of enzymatic performance on stirring speed was observed. Under orbital agitation, the activity of the immobilized CALB progressively increased from 20 up to 150 rpm, suggesting that moderate turbulence promotes efficient mass transfer, better distribution of the magnetic nanoparticles, and enhanced enzyme-support contact. However, further increases in agitation beyond 150 rpm led to a notable decline in catalytic performance, with activity losses becoming significant at 200 and 250 rpm. This trend indicates that, although mild stirring facilitates covalent bonding by increasing molecular collisions, excessive shear introduces mechanical stresses that outweigh the kinetic benefits.

The comparison between orbital and rotational agitation revealed that the latter provided a more stable hydrodynamic regime, with less localized turbulence and reduced interfacial shear. Consequently, under rotational stirring, enzyme immobilization exhibited superior performance at the tested speeds. The derivative activity increased as stirring was raised from 20 to 45 rpm, achieving a maximum value of 28 ± 0.5 U $g^{-1}$ at 45 rpm. This condition was selected as optimal for subsequent experiments. In contrast, orbital agitation at 250 rpm caused a sharp drop in derivative activity, confirming that elevated shear rates can disrupt the tertiary structure of the enzyme and compromise catalytic function.

Mechanistically, this behavior can be interpreted as a balance between mass-transfer enhancement and mechanical denaturation. At low stirring speeds, enzyme-support collisions are insufficient for efficient immobilization; at excessively high speeds, the mechanical energy transmitted through liquid shear and microbubble formation leads to partial unfolding or detachment of the enzyme from the nanoparticle surface.[51] For nonporous materials such as APTS/GLU-functionalized magnetite, these effects are amplified because the enzyme is immobilized on an exposed surface rather than within protective pores, leaving it fully susceptible to hydrodynamic stress.[52] Thus, agitation exerts a dual effect-kinetic and structural-that must be carefully optimized to maintain catalytic integrity.

These findings emphasize that hydrodynamic conditions should be regarded as an intrinsic parameter of the immobilization design, rather than a mere operational variable. The optimal agitation regime (45 rpm, rotational stirring) achieved a favorable compromise between diffusion enhancement and structural preservation of CALB. Under these conditions, the covalent cross-linking proceeded efficiently, forming a uniform enzyme layer without promoting denaturation. This optimized setup was therefore adopted for all subsequent immobilization and biocatalytic assays.

## Biocatalytic study

### Effect of enzyme loading

The relationship between enzyme loading and catalytic performance was investigated to determine the optimal theoretical activity ($A_{to}ff$) for CALB immobilization on the MNs support. The tested loading range varied from 45 to 200 U $g^{-1}$, and the resulting derivative activities and immobilization yields are shown in Figure 8.

Enzyme loading is a key determinant of biocatalyst performance, as it dictates the surface density of active sites and the degree of intermolecular interaction among immobilized enzymes. At lower loadings, the nanoparticle surface may not be fully saturated, leading to underutilization of available binding sites. Conversely, excessively high loadings can cause steric crowding and restricted substrate diffusion, especially in nanostructured systems where enzymes compete for limited accessible area. The systematic evaluation of $A_{to}ff$ thus provides crucial insight into how surface coverage affects both the catalytic efficiency and operational stability of the immobilized CALB.

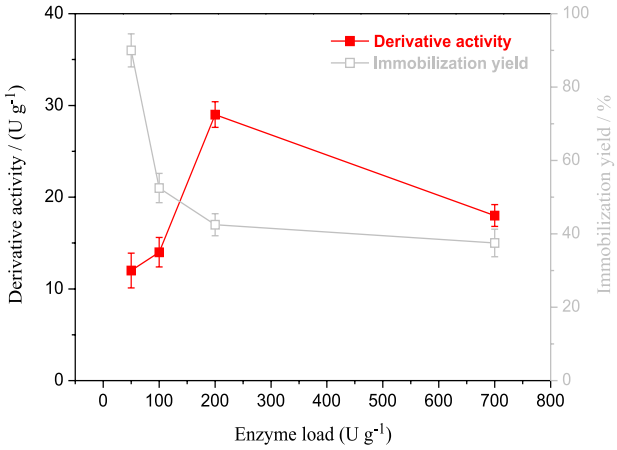


**Figure 8.** Effect of enzyme load ($A_{to}ff$, U $g^{-1}$) on immobilization of lipase B from *Candida antarctica* (CALB) in MNs (magnetic nanoparticles). (■) Derivative activity (U $g^{-1}$) and (□) Immobilization yield (%). The lines represent the trend of experimental data.

As shown in Figure 8, increasing the enzyme loading up to 80 U $g^{-1}$ led to a marked rise in the catalytic activity of the immobilized CALB, reaching a maximum value of 29.1 ± 0.9 U $g^{-1}$. This behavior reflects the progressive occupation of available reactive sites on the magnetic nanoparticle surface, which enhances the density of active catalytic centers and facilitates more efficient substrate turnover. However, further increases beyond this optimal loading threshold resulted in a clear decline in derivative activity, suggesting that excessive enzyme concentration exerts an adverse effect on overall catalytic performance.

The decline in activity at high loading levels can be attributed to several interrelated phenomena. The most immediate explanation involves protein-protein interactions that occur when enzyme molecules are immobilized too densely on the carrier surface. Under such molecular crowding conditions, adjacent CALB molecules may experience steric hindrance or electrostatic repulsion that restricts substrate access to the active site. Moreover, intermolecular interactions can distort enzyme orientation, masking the catalytic domain and leading to conformational strain. These spatial constraints hinder efficient diffusion of substrates and products, causing apparent activity loss despite the presence of more enzyme molecules.

Beyond simple steric effects, high surface crowding can induce conformational alterations due to partial unfolding or rigidification of surface-exposed residues, as the natural hydration shell and local flexibility of the enzyme become perturbed. Such conformational stress can modify the dynamic behavior of the enzyme's active-site lid, particularly relevant for lipases, whose catalytic efficiency depends on maintaining a delicate balance between open and closed conformations. Additionally, dense enzyme packing may alter the physicochemical microenvironment-affecting pH, polarity, and ionic distribution near the nanoparticle surface-which in turn influences catalytic turnover rates.

It is therefore evident that increasing enzyme loading does not guarantee improved performance; beyond an optimal value, the system enters a diffusion-limited regime where internal or external mass-transfer constraints dominate the overall kinetics. Under these conditions, substrates struggle to access buried active sites, and product release becomes hindered, resulting in a measurable drop in apparent activity. Thus, enzyme crowding and restricted molecular mobility act synergistically to reduce efficiency at higher loadings.[53]

Optimizing enzyme loading is therefore a critical engineering parameter in the design of immobilized biocatalysts. It requires striking a balance between achieving sufficient surface coverage for mechanical stability and preserving the conformational freedom necessary for catalytic function. The optimal loading identified at 80 U $g^{-1}$ represents this compromise-providing enough enzyme molecules to fully exploit the functionalized surface while avoiding the detrimental effects of over-saturation. This result aligns with previous studies reporting that excessive immobilization density leads to self-inhibition and reduced substrate accessibility in nanostructured enzyme systems.

### Effect of enzyme-support contact time on enzyme immobilization

The influence of the enzyme-support contact time on immobilization efficiency and catalytic activity was subsequently analyzed, and the results are summarized in Figure 9. By correlating immobilized protein content with derivative activity, it was possible to determine the optimal incubation duration required to achieve maximum enzyme loading without compromising structural integrity or catalytic function. The next section explores how the balance between kinetic attachment and conformational stability evolves over time, providing essential insight into the dynamics of the immobilization process.

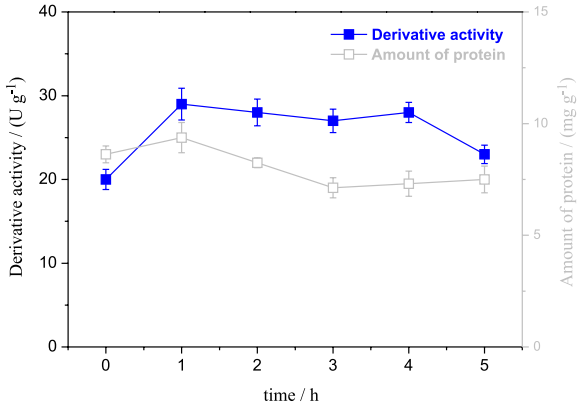


**Figure 9.** Effect of contact time on enzyme immobilization. (■) Derivative activity (U $g^{-1}$). (□) Amount of protein (mg $g^{-1}$). The lines represent the trend of experimental data.

As shown in Figure 9, the amount of protein immobilized on the magnetic nanoparticles remained nearly constant over the tested time interval, indicating that the enzyme-support interaction occurs rapidly and reaches equilibrium within the first hour. The highest catalytic activity of the immobilized CALB was achieved at this point (1 h), confirming that the covalent attachment and conformational adaptation of the enzyme to the APTS/GLU-functionalized surface proceed efficiently in a relatively short period. Beyond this optimal time, however, a gradual decline in activity of approximately 20-25% was observed after 4 h of incubation.

This loss of activity after extended contact likely arises from excessive enzyme-support interactions, which can promote partial conformational rearrangements or over-rigidification of the enzyme's tertiary structure.[53] When the immobilization period is prolonged, multipoint covalent attachments may increase to the point that the enzyme's structural flexibility-particularly near the active-site region-is restricted. Such structural tightening can hinder the dynamic motions necessary for substrate binding and product release, thereby reducing overall

catalytic efficiency. In lipases, whose activity depends on subtle movements of the active-site lid, these effects are especially pronounced; excessive cross-linking may "lock" the enzyme in less active conformations or alter the orientation of catalytic residues.

The rapid immobilization observed within one hour reflects the synergistic contribution of multiple interaction mechanisms operating simultaneously in the system. Initially, covalent bonding via glutaraldehyde provides strong anchoring between the enzyme's amino groups and the activated surface. In parallel, interfacial activation facilitates the adsorption of CALB onto hydrophobic domains of the functionalized nanoparticles, aligning the enzyme in a catalytically favorable orientation. Ionic exchange interactions may also contribute, given the presence of amine and carboxyl groups on both enzyme and carrier, stabilizing early enzyme-support associations before covalent fixation occurs.

Another factor contributing to this rapid and efficient immobilization is the nonporous nature of the support, which eliminates intraparticle diffusion barriers and allows unrestricted enzyme access to reactive surface sites. This structural openness favors direct contact between enzyme molecules and the glutaraldehyde-activated surface, promoting quick saturation of binding sites and high immobilization yield.

Altogether, these results demonstrate that the immobilization of CALB onto the APTS/GLU-functionalized magnetic nanoparticles is a kinetically fast and structurally efficient process. The optimal contact time of one hour offers the best compromise between enzyme anchoring and conformational preservation, ensuring high catalytic activity and reproducibility of the immobilization protocol. The corresponding immobilization parameters obtained under these conditions are summarized in Table 1, which serves as a reference for the subsequent biocatalytic analyses.

Lish *et al.*[54] investigated the catalytic performance of CALB immobilized on magnetic nanoparticles and reported an immobilization yield of approximately 82% after 24 h of incubation. In contrast, the present study achieved a comparable immobilization profile within just one hour, representing a significant improvement in process kinetics. This finding suggests that the functionalization route adopted here-APTS silanization followed by glutaraldehyde activation-provides a highly reactive surface that promotes rapid covalent attachment of enzyme molecules. The ability to attain substantial enzyme loading in a fraction of the time required by traditional methods directly enhances process efficiency and scalability, both of which are essential for industrial biocatalysis.

**Table 1.** Immobilization parameters of magnetic nanoparticles (MNs) and the biocatalyst MNs-CALB (lipase B from *Candida antarctica* immobilized on magnetite functionalized in APTS and activated with glutaraldehyde): including the actual activity of the derivative, immobilization yield, theoretical activity, and recovered activity

| Immobilization parameter | Biocatalyst (MNs-CALB) |
|---|---|
| Derivative activity / (U $g^{-1}$) | 29 ± 0.91 |
| Immobilization yield / % | 75 ± 0.13 |
| Theoretical activity / (U $g^{-1}$) | 59 ± 0.23 |
| Efficiency / % | 46 ± 0.19 |

Monteiro *et al.*[55] similarly explored the immobilization of CALB on magnetic nanoparticles functionalized with APTES and activated with glutaraldehyde. They reported an immobilization yield of 38.2%, closely matching the 29% yield obtained in the present work under optimized conditions. The slight difference in performance can be attributed to variations in surface chemistry, particle morphology, and the density of amine groups available for cross-linking. These comparisons collectively validate the robustness of our immobilization protocol and highlight how subtle differences in synthesis parameters-such as solvent polarity, activation time, or glutaraldehyde concentration-can markedly influence enzyme orientation and covalent binding efficiency.

The rapid immobilization behavior observed here-characterized by high catalytic activity at early stages followed by partial loss upon prolonged contact-corroborates the findings of other studies involving aldehyde-functionalized supports. For example, in the immobilization of *Serratia marcescens* lipase on APTS-coated $Fe_3O_4$ nanoparticles, nearly complete enzyme binding occurred within 10 min, with longer incubation (up to 120 min) yielding no further improvement.[56] This parallels our results, demonstrating that the primary binding events between the enzyme and the glutaraldehyde-activated surface are extremely fast, driven by strong aldehyde-amine condensation reactions. After this initial stage, additional contact time mainly contributes to excessive cross-linking or conformational tightening, which may reduce catalytic flexibility.

Conversely, *Thermomyces lanuginosus* lipase immobilized on aldehyde-functionalized APTS-$Fe_3O_4$ nanoparticles required approximately two hours to reach optimal immobilization, after which the enzyme maintained high activity and stability over extended use.[57] This difference illustrates how enzyme structure and lid dynamics influence immobilization kinetics: while CALB exhibits a compact, relatively rigid active site that favors fast covalent anchoring, lipases with larger, more mobile lids (such as *T. lanuginosus*) may require

longer incubation times to achieve optimal orientation and cross-linking.

Taken together, these literature comparisons reinforce the interpretation that the immobilization of CALB onto APTS/GLU-modified magnetic nanoparticles is governed primarily by covalent attachment mechanisms, which proceed rapidly and efficiently. However, these same strong binding interactions introduce a kinetic-structural trade-off: extending the incubation time beyond the optimal range enhances multipoint linkage density but simultaneously restricts conformational freedom, leading to the gradual loss of activity observed after prolonged contact. This delicate equilibrium between immobilization extent and structural preservation underscores the importance of precise temporal control during biocatalyst preparation.

## Reuse of the immobilized enzyme

Given that reusability is a cornerstone of industrial biocatalyst design, the operational stability of the MNs-CALB derivatives was evaluated across multiple reaction cycles. Figure 10 presents the hydrolytic activity profiles over successive batch runs for derivatives prepared under varying enzyme-support contact times. The progressive decline in activity with reuse provides quantitative insight into how immobilization conditions influence mechanical robustness and covalent stability under repetitive operational stress.

The results revealed that the derivatives prepared under optimized conditions (1 h contact time, 45 rpm rotational stirring) exhibited the highest retention of catalytic activity across cycles, confirming that the immobilization strategy yields a biocatalyst that is both structurally resilient and magnetically recoverable. Conversely, derivatives subjected to longer immobilization periods showed a steeper activity decay, consistent with the earlier observation that excessive cross-linking and over-rigidification reduce the conformational elasticity needed for repeated catalysis. The trends observed here mirror industrial expectations: maximizing the number of reusable cycles without significant loss of activity is key to reducing process costs and improving overall sustainability.

In summary, these findings demonstrate that careful optimization of immobilization kinetics and hydrodynamic conditions can produce CALB-based magnetic biocatalysts with a desirable combination of rapid preparation, high catalytic efficiency, and excellent reusability-a triad of properties essential for integrating enzymatic nanomaterials into continuous or semi-continuous bioprocesses.

The biocatalyst prepared under the optimized immobilization conditions-1 h of enzyme-support contact

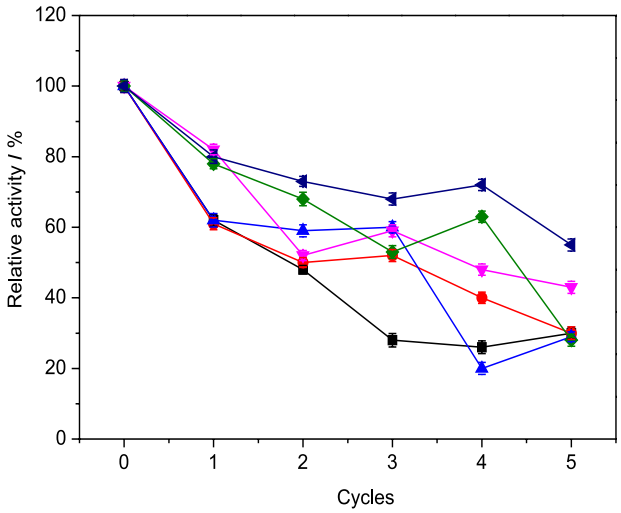


**Figure 10.** Operational stability in the hydrolysis of p-NPB (p-nitrophenyl butyrate) by MNs-CALB (lipase B from Candida antarctica immobilized on magnetite functionalized with APTS and activated with glutaraldehyde). Relative activity (%) as a function of reuse cycles for derivatives prepared at different enzyme–support contact times: black line with square symbols (■) 30 min; red line with circle symbols (●) 1 h; blue line with triangle symbols (▲) 2 h; green line with rhombus symbols (◆) 3 h; magenta line with triangle symbols (▼) 4 h; and dark-blue line with triangle symbols (▲) 5 h. The lines represent the trend of the experimental data.

time-displayed the most favorable hydrolytic performance and reusability profile. As shown in Figure 10, this derivative retained approximately 50% of its initial activity after six consecutive catalytic cycles, demonstrating notable structural integrity and operational robustness under repeated use. The ability of the MNs-CALB system to maintain half of its original activity over multiple cycles confirms the effectiveness of the covalent bonding achieved through glutaraldehyde activation, which minimizes enzyme leaching and mechanical detachment during reaction and recovery.

This level of reusability is highly competitive when compared with conventional immobilization systems reported in the literature for CALB and other lipases, where activity losses often exceed 60-70% after only three to four cycles. The results therefore underscore the strength of the enzyme-support interface produced in this study, in which the APTS-GLU functional layer ensures both stable attachment and preservation of catalytic functionality. Moreover, the moderate activity decline observed is likely attributed to cumulative conformational fatigue or minor microenvironmental changes during repeated washing and handling steps, rather than to chemical desorption.

Based on these results, all subsequent preparations of MNs-CALB derivatives were standardized to 1 h of immobilization time, as this condition provided the best compromise between high initial activity, mechanical stability, and long-term operational performance. This

optimized configuration was thus adopted as the reference for further analyses of structural and thermal behavior.

### Thermal stability of soluble and immobilized CALB

The thermal stability profiles of both soluble and immobilized CALB were examined under controlled conditions at 60 °C and pH 7.0 in a 25 mM sodium phosphate buffer for a 48-h incubation period. The results, presented in Figure 11, clearly reveal distinct thermal inactivation patterns between the free and immobilized enzymes, reflecting the protective effect conferred by immobilization.

The soluble enzyme exhibited a rapid loss of catalytic activity within the first few hours of incubation, consistent with the known thermal sensitivity of CALB in aqueous environments. The lack of structural constraints in the soluble form allows thermal agitation to disrupt intramolecular hydrogen bonds and destabilize the hydrophobic core, leading to irreversible unfolding and deactivation. In contrast, the immobilized CALB demonstrated a markedly slower rate of inactivation, maintaining a substantial fraction of its original activity even after prolonged exposure to elevated temperature. This enhanced thermostability arises from the multipoint covalent attachment and restricted conformational mobility imparted by the APTS/GLU-functionalized magnetic support. The immobilization effectively "locks" the enzyme in a more rigid configuration, which reduces the entropy associated with unfolding transitions and stabilizes key catalytic residues within the active site.

Moreover, the magnetic carrier may contribute to additional microenvironmental stabilization by moderating local polarity and providing a less hydrated interfacial region around the enzyme, thereby reducing water-induced denaturation processes. Collectively, these effects illustrate how the designed immobilization strategy successfully transforms CALB into a structurally reinforced and thermally resilient biocatalyst, capable of sustaining catalytic activity under conditions that would normally inactivate the soluble enzyme.

The comparative analysis of the thermal inactivation profiles (Figure 11) revealed a pronounced difference between the soluble and immobilized forms of CALB. The soluble enzyme underwent rapid deactivation, losing over 70% of its initial activity within the first 6 min of exposure at 60 °C. This steep decline reflects the high conformational sensitivity of CALB in its free state, where the lack of structural confinement allows thermal agitation to disrupt the delicate hydrogen-bonding and hydrophobic interactions that stabilize the native fold. Once unfolded, the exposed hydrophobic residues promote irreversible aggregation and rapid catalytic loss.

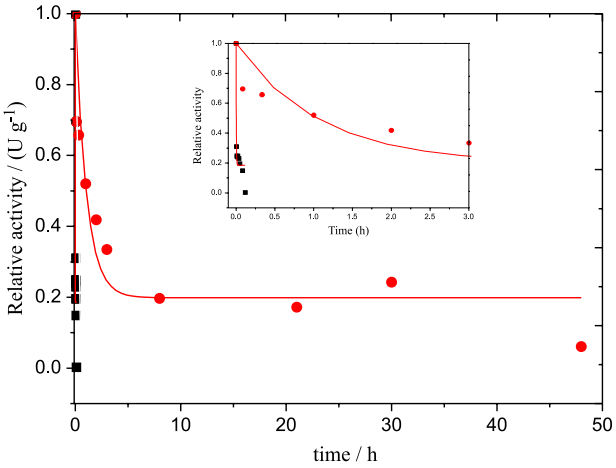


**Figure 11.** Thermal stability of CALB-soluble (lipase B from *Candida antarctica*) and MNs-CALB derivatives at 60 °C and pH 7. Soluble enzyme Att = 93 U $mL^{-1}$ and MNs-CALB derivatives (lipase B from *Candida antarctica* immobilized on magnetite functionalized in APTS and activated with glutaraldehyde) Att = 80 U $g^{-1}$. Relative activity: (●) immobilized CALB and (■) CALB soluble. The lines represent the trend of the Sadana and Henley models.

In contrast, the immobilized enzyme displayed significantly enhanced thermal resistance, losing only about 20% of its initial activity during the same period. Remarkably, even after 20 h, the immobilized CALB retained approximately 20% of its initial activity, confirming that the immobilization matrix confers a pronounced protective effect. This stability enhancement can be attributed to multiple synergistic factors:

(*i*) Multipoint covalent attachment via glutaraldehyde restricts large-scale conformational motions, lowering the entropy of unfolding transitions;

(*ii*) Surface confinement within the APTS/GLU network reduces the probability of intermolecular aggregation; and

(*iii*) Microenvironmental modulation, in which the local polarity and hydration around the enzyme are altered, creating a semi-rigid microdomain that buffers thermal perturbations.

Collectively, these effects transform CALB from a thermolabile enzyme into a thermotolerant biocatalyst capable of sustained operation at temperatures where the soluble form is rapidly denatured. Such an enhancement is particularly relevant for industrial hydrolytic or transesterification processes that demand prolonged exposure to elevated temperatures to increase reaction rates or reduce medium viscosity.

The quantitative thermal deactivation data are summarized in Table 2, which lists the half-life ($t_{1/2}$) and stabilization factor (SF) for both soluble and immobilized forms at 60 °C. The immobilization process resulted in a dramatic improvement of the enzyme's thermal robustness,

with $t_{1/2}$ increasing from 3 min (soluble CALB) to 60 min (MNs-CALB)-a 20-fold enhancement in stability. This substantial rise in half-life unequivocally demonstrates that covalent immobilization on the APTS/GLU-modified magnetic nanoparticles effectively shields CALB from thermal denaturation and aggregation. The stabilization factor (SF > 1) further corroborates that immobilization not only preserves enzyme activity but also redefines its kinetic resistance to temperature-induced inactivation.

In summary, these findings confirm that the immobilized CALB derivative exhibits a thermodynamically stabilized structure with reduced conformational entropy, enabling prolonged activity retention under harsh operational conditions. This thermal reinforcement, combined with the catalyst's demonstrated reusability, highlights its potential as a durable and recyclable biocatalyst for high-temperature bioprocesses in the chemical, food, and pharmaceutical sectors.

**Table 2.** Thermal deactivation at 60 °C and pH 7 of soluble CALB (lipase B from *Candida antarctica*) and MNs-CALB (lipase B from *Candida antarctica* immobilized on magnetite functionalized in APTS and activated with glutaraldehyde) derivatives

| Biocatalyst | Kd / $h^{-1}$ | $t_{1/2}$ / h | Stabilization factor (SF) |
|---|---|---|---|
| Soluble CALB | 15.3 ± 366 | 0.051 | – |
| CALB-IMNS | 0.94 ± 18 | 1.0 | 20.0 |

Kd: deactivation rate constant; $t_{1/2}$: half-life; CALB-IMNS: *Candida antarctica* lipase B immobilized on magnetic nanoparticles.

The immobilized CALB exhibited a 20-fold increase in stability at 60 °C compared to its soluble counterpart, as indicated by the significantly higher SF. This pronounced improvement reflects the conformational restrictions imposed by multipoint covalent attachment, which minimize thermal fluctuations and protect the tertiary structure of the enzyme. In its soluble state, CALB possesses substantial conformational flexibility; while this flexibility is beneficial for substrate accommodation under mild conditions, it also renders the active site susceptible to irreversible unfolding at elevated temperatures. Upon immobilization, however, the enzyme becomes structurally reinforced: the formation of covalent bonds between surface lysine residues and the glutaraldehyde-activated APTS support generates a semi-rigid molecular scaffold that stabilizes the catalytic domain and preserves the geometry of the active site even under thermal stress.

The stabilization effects observed in the immobilized CALB can be attributed to both intermolecular cross-linking (enzyme-support bonds) and intramolecular conformational tightening within the enzyme itself.[58] These interactions reduce the entropy of unfolding and protect critical structural motifs such as the α-helix surrounding the catalytic Ser[105] and the oxyanion hole that stabilizes transition states during catalysis. In essence, immobilization does not merely anchor the enzyme but reshapes its conformational energy landscape toward a more thermodynamically favorable, low-mobility state that resists denaturation.

Comparable stabilization effects have been documented by other researchers. Hu *et al.*[56] reported the thermal deactivation of soluble and immobilized CALB on modified chitosan supports at 60 °C, obtaining half-lives between 1.0 and 3.3 h for the immobilized forms, representing 12-33-fold improvements in stability relative to the soluble enzyme. Similarly, Monteiro *et al.*[55] examined the thermal behavior of immobilized lipases and reported enhanced stability when compared to their soluble counterparts. Despite the lower temperature optimum, the immobilized enzyme retained its activity across a broader operational window (45-55 °C), reflecting greater structural robustness and slower deactivation kinetics.

These findings align closely with the results obtained in the present work, confirming that the APTS/GLU immobilization strategy effectively reproduces the protective effects seen in other hybrid systems. The enhanced thermostability observed here arises from a synergistic interplay between chemical cross-linking, microenvironmental modification, and molecular confinement. Together, these mechanisms underpin the superior durability of the MNs-CALB biocatalyst, making it an attractive candidate for high-temperature or long-duration industrial applications.

### Enantioselective esterification of racemic ibuprofen

To assess the catalytic performance and enantioselectivity of the immobilized enzyme, the MNs-CALB derivative was applied to the esterification of racemic ibuprofen with 1-propanol in cyclohexane. This reaction represents a benchmark test for lipase enantioselectivity and is particularly relevant to pharmaceutical synthesis, where the separation of *R*- and *S*-ibuprofen enantiomers determines both therapeutic efficacy and safety.

For comparison, identical reaction conditions were applied to the commercial biocatalyst Novozym 435, a well-established CALB preparation immobilized on a macroporous acrylic resin. The esterification rate (percentage of conversion) for both systems, summarized in Table 3, provides a direct measure of catalytic efficiency and stereochemical discrimination under equivalent operational environments. This comparative evaluation enables the quantitative assessment of how the custom magnetic derivative (MNs-CALB) performs relative to a

commercial benchmark in terms of both reaction kinetics and enantioselective bias.

Beyond its intrinsic catalytic relevance, this experiment also serves to validate the functional integrity of the immobilized CALB after chemical modification and thermal stabilization. Demonstrating comparable or superior enantioselectivity relative to Novozym 435 underlines that the immobilization process preserved the enzyme's chiral recognition capability-an essential criterion for its application in asymmetric synthesis and the manufacture of optically pure pharmaceuticals.

**Table 3.** Esterification of racemic ibuprofen catalyzed by different immobilized lipases[a]

| Biocatalyst | time / h | Conversion / % |
|---|---|---|
| Novozym® | 24 | 69.00 |
| | 48 | 98.00 |
| | 72 | 99.40 |
| MNs-CALB[b] | 24 | 2.84 |
| | 48 | 4.59 |
| | 72 | 25.00 |

[a]Reaction medium: racemic ibuprofen and 1-propanol (1:3, acid/alcohol) in organic medium (cyclohexane) at 37 °C (600 rpm) for 72 h. Immobilized enzyme activity *per* gram of support of 29.1 g using 80 U*p*-NPB $g^{-1}$ enzyme load. [b]MNs-CALB (lipase B from *Candida antarctica* immobilized on magnetite functionalized in APTS and activated with glutaraldehyde) derivatives.

As shown in Table 3, the time-course analysis of racemic ibuprofen esterification revealed distinct kinetic behaviors for the two immobilized enzyme systems. In the case of Novozym 435, aliquots collected at 24, 48, and 72 h confirmed the progressive formation of (*R*,*S*)-ibuprofen propyl ester, with the highest conversion occurring at 48 h. This profile is consistent with the known high accessibility and hydrophobic environment provided by the macroporous acrylic resin used in Novozym 435, which facilitates efficient substrate diffusion and product desorption in organic media.

In contrast, the custom MNs-CALB derivative exhibited a slower but steady reaction progression, achieving its maximum conversion of approximately 25% at 72 h. Although this value is lower than that achieved by the commercial preparation, the kinetic trend reflects a more gradual catalytic behavior, likely influenced by the physicochemical nature of the magnetic nanoparticle surface. The moderate hydrophilicity of the APTS/GLU-functionalized magnetite may limit substrate partitioning at the enzyme-solvent interface, leading to a slower approach to equilibrium. Nonetheless, the continuous and sustained increase in conversion indicates that the enzyme remains catalytically active over extended reaction times without evidence of rapid deactivation-a desirable trait for long-term or continuous-flow applications.

These kinetic differences underline the contrasting operational dynamics of the two systems. Novozym 435, optimized for high initial activity, tends to achieve rapid conversion but may suffer from faster performance decay due to diffusion limitations or partial desorption of enzyme molecules from its organic polymer matrix under prolonged use. In contrast, MNs-CALB displays a more controlled reaction profile, consistent with strong covalent anchoring and enhanced structural rigidity, which provide superior operational stability and reusability.

Beyond catalytic efficiency, the magnetic recoverability of MNs-CALB represents a substantial operational advantage. The ability to separate the biocatalyst from the reaction medium within seconds using a simple external magnet eliminates the need for filtration or centrifugation, minimizing product contamination and enzyme loss. This feature not only simplifies downstream processing but also significantly reduces operational costs and enhances the purity of the final product, which is critical for pharmaceutical-grade syntheses. Thus, while the conversion yield of MNs-CALB is slightly lower, its ease of recovery, recyclability, and process integration potential present tangible benefits for sustainable biocatalytic manufacturing.

Moreover, these findings align with literature reports emphasizing the superior efficiency of immobilized *versus* soluble lipases under similar esterification conditions. Ferreira *et al.*[57] investigated the performance of soluble lipases for racemic ibuprofen esterification with 1-propanol and observed no detectable product formation within 24-72 h.[59] In their study, the reaction only initiated after approximately 100 h, yielding 20 and 12% of (*R*,*S*)-ibuprofen propyl ester after 250 h of reaction. In stark contrast, the immobilized CALB derivatives-both Novozym 435 and MNs-CALB-achieved comparable or higher conversions within one-third of that time frame.

These results unequivocally demonstrate that immobilization not only enhances enzyme stability but also accelerates reaction kinetics, even under non-aqueous conditions. The MNs-CALB system, in particular, combines catalytic competence with magnetic responsiveness, yielding a versatile and reusable nanobiocatalyst that meets the growing demand for efficient, clean, and easily recoverable enzymatic systems in fine chemical and pharmaceutical production.

### Molecular docking

To gain molecular-level insights into the stereochemical preferences observed experimentally, molecular docking

simulations were performed following previously reported methodologies,[60] with specific adaptations to the present system.[61] This computational study aimed to elucidate the binding interactions and energetic behavior of both enantiomers-(*R*)-(−)-ibuprofen and (*S*)-(+)-ibuprofen-within the active site of CALB.

Docking analyses provide a predictive framework for understanding how molecular orientation, steric accommodation, and hydrogen-bonding interactions govern the enantioselective esterification mechanism catalyzed by CALB. The active site of the enzyme, located in a shallow hydrophobic pocket near the catalytic triad ($Ser^{105}$-$His^{224}$-$Asp^{187}$), is known to discriminate between substrate enantiomers through differential stabilization of transition states and orientation of the carboxyl moiety.

The results, summarized in Table 4, present the binding affinity energies (ΔG, kcal $mol^{-1}$) and RMSD values for each enantiomer-enzyme complex. These parameters quantify both the thermodynamic stability of the binding interaction and the conformational reliability of the predicted docking poses. Lower binding energies indicate stronger affinity and a higher likelihood of productive catalysis, while RMSD values close to or below 2.0 Å confirm the geometric consistency and precision of the docking results.

By comparing the docking outcomes for (*R*) and (*S*)-ibuprofen, it is possible to correlate the observed experimental enantioselectivity with molecular recognition phenomena at the catalytic interface. The analysis also enables visualization of key hydrogen bonds, hydrophobic contacts, and electrostatic interactions between ibuprofen and the catalytic residues of CALB, offering a structural explanation for the preferential conversion behavior of the enzyme.

**Table 4.** Molecular docking result with its dock scores

| Compound | Energy affinity / (kcal $mol^{-1}$) | RMSD / Å | Lipase |
|---|---|---|---|
| (*R*)-(−)-Ibuprofen | −6.8 | < 2.0 | CALB |
| (*S*)-(+)-Ibuprofen | −5.9 | < 2.0 | |

CALB: lipase B from *Candida antarctica*; RMSD: root mean square deviation.

Thus, the molecular docking investigation complements the experimental esterification results, bridging macroscopic performance and microscopic mechanism. The integration of computational and experimental data strengthens the mechanistic understanding of the enantioselective biocatalysis process catalyzed by MNs-CALB, reinforcing the rational design and optimization of next-generation immobilized enzyme systems for chiral synthesis.

The docking simulations revealed comparable RMSD values for (*R*)-(−)-ibuprofen and (*S*)-(+)-ibuprofen, indicating that both enantiomers can adopt stable and well-defined conformations within the CALB active site. However, the binding affinity energies (−6.8 kcal $mol^{-1}$ for the (*R*)-enantiomer and −5.9 kcal $mol^{-1}$ for the (*S*)-enantiomer) highlight a distinct thermodynamic preference for the (*R*)-form. This difference, though subtle, reflects more favorable molecular interactions that stabilize the (*R*)-ibuprofen-CALB complex, consistent with the experimentally observed enantioselectivity during esterification.

The enhanced affinity of (*R*)-ibuprofen can be attributed to a more optimal spatial orientation of its carboxyl and aromatic moieties within the hydrophobic pocket that surrounds CALB's catalytic triad. This orientation promotes stronger hydrogen bonding and van der Waals interactions with residues lining the active site, enabling tighter substrate anchoring and more efficient transition-state stabilization. Specifically, the carboxyl group of (*R*)-ibuprofen forms favorable electrostatic interactions with the oxyanion hole, typically involving Thr40 and Gln106, which stabilize the negatively charged tetrahedral intermediate during catalysis. In contrast, the (*S*)-enantiomer adopts a slightly less favorable orientation, resulting in weaker hydrogen-bond geometry and reduced electronic complementarity.

Consistent with the canonical mechanism of serine hydrolases, CALB's catalytic triad-composed of Ser105, His224, and Asp187 (Figure 12)-plays a central role in facilitating the nucleophilic attack on the substrate's carbonyl carbon.[43] The docking results confirm that both enantiomers are positioned within the same catalytic pocket, yet only the (*R*)-ibuprofen aligns in a geometry that maximizes productive interactions with Ser105's hydroxyl group, favoring acyl-enzyme intermediate formation and subsequent esterification with 1-propanol.

Beyond hydrogen bonding, hydrophobic and alkyl-like interactions further contribute to the binding stabilization of the (*R*)-enantiomer. Key residues, including Ile189 (5.10 Å), Ala141 (4.47 Å), Leu144, and Val154, form a compact hydrophobic cluster that accommodates the aromatic ring and alkyl chain of the ibuprofen, promoting tighter packing within the hydrophobic channel of the enzyme. This spatial complementarity explains the slightly stronger ΔG value for the (*R*)-enantiomer, as these nonpolar contacts minimize solvent exposure and strengthen the overall binding energy through dispersion forces.

Taken together, the docking analysis provides a molecular rationale for CALB's enantioselectivity in racemic ibuprofen esterification. The combination of

stronger hydrogen bonding within the oxyanion hole, optimized orientation toward the catalytic Ser105, and enhanced hydrophobic complementarity with residues such as Ile189, Ala141, Leu144, and Val154 collectively favor the conversion of (*R*)-ibuprofen. These findings establish a clear correlation between the computational and experimental results, demonstrating that binding energy differentials of less than 1 kcal $mol^{-1}$ can decisively influence stereochemical outcomes in enzyme-catalyzed reactions.

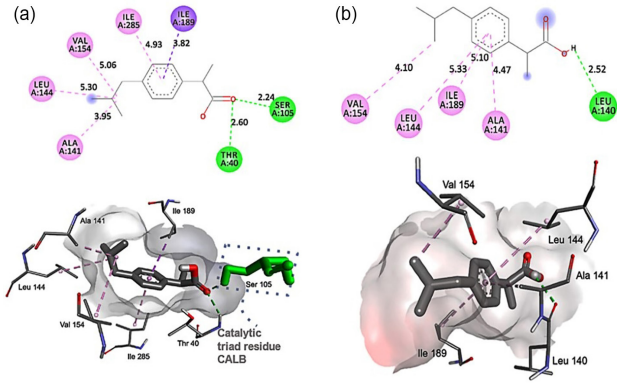


**Figure 12.** Three-dimensional representations of molecular docking studies of CALB with (a) (*R*)-(−)-ibuprofen, including both 2D and 3D views. The active site of CALB (lipase B from *Candida antarctica*) lipase is represented as sticks, featuring the catalytic Ser105 in green. (b) 2D and 3D representations of CALB docked with (*S*)-(+)-ibuprofen.

In this context, each docking pose was carefully analyzed to identify productive conformations-that is, those in which the substrate is positioned within a Near Attack Conformation (NAC) compatible with nucleophilic attack by the catalytic serine on the electrophilic carbon of the substrate.[62] A NAC is a critical geometric prerequisite for catalysis, representing a pre-transition-state arrangement in which the reactive atoms are correctly oriented for bond formation. In typical serine hydrolases such as CALB, the distance between the oxygen of Ser105 and the carbonyl carbon of the substrate should approximate 3.0 Å, while the O–C=O angle formed with the carbonyl oxygen generally lies between 60° and 90°, ensuring optimal orbital overlap for nucleophilic attack.[63]

Our computational analysis revealed that, for (*R*)-(−)-ibuprofen, the substrate adopts conformations that approximate this ideal geometry, facilitating the formation of a productive acyl-enzyme intermediate. Among the ten best docking poses, several exhibited weak NAC features, where the Ser105-carbonyl carbon distance slightly exceeded 3.2 Å and the O–C=O angle was below 60° (Figure 12).[64] Although these values deviate modestly from the canonical NAC parameters, they still suggest that the enzyme-substrate complex is geometrically viable and can proceed to catalysis after minor conformational adjustments.

For the (*R*)-enantiomer (Figure 12a), the active-site geometry displayed a rich network of stabilizing interactions that collectively favor the formation of the acyl-enzyme complex. A hydrogen bond between the hydroxyl oxygen of Ser105 and the carboxyl oxygen of the substrate was observed at 2.24 Å, positioning the substrate for nucleophilic attack. An additional hydrogen bond involving Thr40 (2.64 Å) further stabilizes the substrate carbonyl within the oxyanion hole, reducing the activation energy required for acylation. Complementing these polar interactions, several hydrophobic contacts were identified between the substrate's aromatic ring and residues Ile285 (4.93 Å), Val154 (5.06 Å), Leu144 (5.30 Å), and Ala141, which help to anchor the ibuprofen moiety in a catalytically competent orientation. Moreover, a π-σ hydrophobic interaction was observed with Ile189 (3.82 Å), providing additional stabilization through dispersion forces.

In contrast, the (*S*)-(+)-ibuprofen configuration (Figure 12b) failed to establish productive interactions with the catalytic triad (Ser105-His224-Asp187), thereby explaining the low conversion of the *S*-enantiomer observed experimentally. Instead, the (*S*)-form adopted a less favorable orientation, characterized by a single hydrogen bond with Leu140 (2.52 Å)-a residue located outside the principal catalytic pocket. The absence of direct interactions with Ser105 and the oxyanion hole indicates a geometrically misaligned substrate, incapable of efficient acylation or transition-state stabilization.

Taken together, these findings reveal that enantioselectivity arises primarily from geometric and electronic complementarity between (*R*)-ibuprofen and the CALB active site. The (*R*)-enantiomer aligns its carboxyl group within the catalytic pocket to form both hydrogen-bonding and hydrophobic interactions that approximate a NAC, while the (*S*)-form adopts an orientation that is sterically hindered and catalytically unproductive. This molecular distinction corroborates the experimental evidence of preferential formation of (*R*)-(−)-ibuprofen propyl ester, firmly linking docking predictions to observed reaction outcomes.

## Conclusions

The systematic investigation of the experimental parameters demonstrated that the stirring rate, enzyme loading, glutaraldehyde concentration, and contact time exert a decisive influence on the immobilization efficiency and catalytic performance of CALB on $Fe_3O_4$ magnetic nanoparticles. The optimized biocatalyst, prepared under

the conditions of 45 rpm, 80 U $g^{-1}$ enzyme load, 25% glutaraldehyde, and 1 h contact time, exhibited the highest derivative activity (29.1 ± 0.9 U $g^{-1}$). These conditions provided an optimal balance between covalent anchoring and preservation of enzyme conformation.

Physicochemical characterization by VSM, SEM, and FTIR confirmed the successful functionalization of the magnetic nanoparticles and the stable immobilization of CALB on the APTS/GLU-activated surface. The resulting biocatalyst displayed excellent magnetic responsiveness, ensuring rapid and efficient recovery from the reaction medium through simple magnetic separation.

Thermal inactivation studies revealed that immobilization improved the enzyme's thermal stability by approximately 20-fold relative to its soluble form, evidencing that multipoint covalent attachment effectively restricts conformational mobility while maintaining catalytic integrity. This stabilization, combined with consistent reusability over six reaction cycles, highlights the robustness and practical applicability of the immobilized system for industrial biotransformations.

The immobilized CALB was further evaluated in the enantioselective esterification of racemic ibuprofen, confirming its catalytic competence and chiral discrimination capacity. The MNs-CALB derivative achieved 25% conversion at 72 h, with clear preference toward the (*R*)-(−)-ibuprofen enantiomer. Molecular docking analyses corroborated the experimental findings, revealing that the (*R*)-enantiomer establishes multiple productive interactions with CALB's catalytic triad (Ser105-His224-Asp187) and with Thr40 within the oxyanion hole, forming a geometry consistent with a NAC. In contrast, (*S*)-(+)-ibuprofen exhibited no effective alignment with the catalytic residues, explaining its limited conversion.

In summary, this study demonstrates that the APTS/GLU-functionalized $Fe_3O_4$ nanosystem is an efficient and magnetically recoverable support for CALB immobilization, combining high stability, reusability, and enantioselective capability. The integration of experimental and molecular modeling approaches provided comprehensive mechanistic insight into enzyme-substrate interactions, establishing a strong foundation for the rational design of next-generation magnetic nanobiocatalysts aimed at sustainable and selective synthesis of chiral pharmaceuticals.

### Data Availability Statement

All data supporting the findings of this study are included within the article.

### Acknowledgments

The authors acknowledge and thank the financial support of the Fundação Cearense de Apoio ao Desenvolvimento Científico e Tecnológico (FUNCAP, PS1-00186-00216.01.00/21), CNPq (311062/2019-9) and CAPES (Finance Code 001), under the support of the Instituto de Engenharias e Desenvolvimento Sustentável (IEDS), the Universidade da Integração Internacional da Lusofonia Afro-Brasileira (UNILAB), Advanced Materials Chemistry Group (GQMat) at the Federal University of Ceará (UFC) and Biotechnology and Synthesis Laboratory - LABS at the Federal University of Ceará (UFC).

### Author Contributions

M.C.M.S. was responsible for conceptualization, methodology, writing review and editing, visualization and supervision, project administration, funding acquisition; L.R.B.G. for conceptualization; P.B.A.F. for methodology; J.F.S. for validation, investigation, writing (original draft preparation, review and editing); A.M. F. for software; J. F.-L. writing review and editing; J.C.S.S. for writing (review and editing), visualization and supervision.

## References

1. Wagner, K.; Hummel, A.; Yang, J.; Horino, S.; Kanomata, K.; Akai, S.; Gröger, H.; *ChemBioChem* **2024**, *25*, e202400082. [Crossref]
2. Hasan, F.; Shah, A. A.; Hameed, A.; *Enzyme Microb. Technol.* **2006**, *39*, 235. [Crossref]
3. Parandi, E.; Safaripour, M.; Mosleh, N.; Saidi, M.; Rashidi Nodeh, H.; Oryani, B.; Rezania, S.; *Biomass Bioenergy* **2023**, *173*, 106794. [Crossref]
4. Lv, D.; Wang, M.; He, W.; Wu, J.; Liu, X.; Guan, Y.; *Food Chem.* **2023**, *421*, 136132. [Crossref]
5. McCabe, R. W.; Rodger, A.; Taylor, A.; *Enzyme Microb. Technol.* **2005**, *36*, 70. [Crossref]
6. Bilal, M.; Zhao, Y.; Rasheed, T.; Iqbal, H. M. N.; *Int. J. Biol. Macromol.* **2018**, *120*, 2530. [Crossref]
7. Xing, M.; Chen, Y.; Dai, W.; He, X.; Li, B.; Tian, S.; *J. Hazard. Mater.* **2023**, *448*, 130986. [Crossref]
8. Ruiz-Hernández, E.; López-Noriega, A.; Arcos, D.; Vallet-Regí, M.; *Solid State Sci.* **2008**, *10*, 421. [Crossref]
9. Fernandez-Lopez, L.; Pedrero, S. G.; Lopez-Carrobles, N.; Gorines, B. C.; Virgen-Ortíz, J. J.; Fernandez-Lafuente, R.; *Enzyme Microb. Technol.* **2017**, *98*, 18. [Crossref]
10. Andrade, L. H.; Rebelo, L. P.; Netto, C. G. C. M.; Toma, H. E.; *J. Mol. Catal. B: Enzym.* **2010**, *66*, 55. [Crossref]
11. Netto, C. G. C. M.; Andrade, L. H.; Toma, H. E.; *Tetrahedron: Asymmetry* **2009**, *20*, 2299. [Crossref]
12. Kim, M. H.; Lee, S. B.; Ryu, D. D. Y.; Reese, E. T.; *Enzyme Microb. Technol.* **1982**, *4*, 99. [Crossref]

13. Bai, S.; Guo, Z.; Liu, W.; Sun, Y.; *Food Chem.* **2006**, *96*, 1. [Crossref]
14. Yousefi, M.; Mohammadi, M.; Habibi, Z.; *J. Mol. Catal. B: Enzym.* **2014**, *104*, 87. [Crossref]
15. Ravelo, M.; Fuente, E.; Blanco, Á.; Ladero, M.; García-Ochoa, F.; *Biochem. Eng. J.* **2015**, *101*, 228. [Crossref]
16. Marszałł, M. P.; Siódmiak, T.; *Catal. Commun.* **2012**, *24*, 80. [Crossref]
17. Siódmiak, T.; Ziegler-Borowska, M.; Marszałł, M. P.; *J. Mol. Catal. B: Enzym.* **2013**, *94*, 7. [Crossref]
18. José, C.; Toledo, M. V.; Briand, L. E.; *Crit. Rev. Biotechnol.* **2016**, *36*, 891. [Crossref]
19. Zhao, D. T.; Xun, E. N.; Wang, J. X.; Wang, R.; Wei, X. F.; Wang, L.; Wang, Z.; *Biotechnol. Bioprocess Eng.* **2011**, *16*, 644. [Crossref]
20. Barreto, A. C. H.; Maia, F. J. N.; Santiago, V. R.; Ribeiro, V. G. P.; Denardin, J. C.; Mele, G.; Carbone, L.; Lomonaco, D.; Mazzetto, S. E.; Fechine, P. B. A.; *Microfluid. Nanofluid.* **2012**, *12*, 677. [Crossref]
21. Silva, J. A.; Macedo, G. P.; Rodrigues, D. S.; Giordano, R. L. C.; Gonçalves, L. R. B.; *Biochem. Eng. J.* **2012**, *60*, 16. [Crossref]
22. de Souza, M. C. M.; dos Santos, K. P.; Freire, R. M.; Barreto, A. C. H.; Fechine, P. B. A.; Gonçalves, L. R. B.; *Braz. J. Chem. Eng.* **2017**, *34*, 681. [Crossref]
23. Kordel, M.; Hofmann, B.; Schomburg, D.; Schmid', R. D.; *J. Bacteriol.* **1991**, *173*, 4836. [Crossref]
24. Sadana, A.; Henley, J. P.; *Biotechnol. Bioeng.* **1987**, *30*, 717. [Crossref]
25. da Fonseca, A. M.; de Freitas, Í. B.; Soares, N. B.; de Araújo, F. A. M.; Gaieta, E. M.; dos Santos, J. C. S.; Sobrinho, A. C. N.; Marinho, E. S.; Colares, R. P.; *Biointerface Res. Appl. Chem.* **2022**, *12*, 5901. [Crossref]
26. Wahl, J.; Freyss, J.; von Korff, M.; Sander, T.; *J. Cheminf.* **2019**, *11*, 53. [Crossref]
27. Petrova, S. S.; Solov'ev, A. D.; *Historia Mathematica* **1997**, *24*, 361. [Crossref]
28. Sutton, R. S.; Maei, H. R.; Precup, D.; Bhatnagar, S.; Silver, D.; Szepesvári, C.; Wiewiora, E.; *ICML '09: Proceedings of the 26th Annual International Conference on Machine Learning* **2009**, 993. [Crossref]
29. Hanwell, M. D.; Curtis, D. E.; Lonie, D. C.; Vandermeersch, T.; Zurek, E.; Hutchison, G. R.; *J. Cheminf.* **2012**, *4*, 17. [Crossref]
30. O'Boyle, N. M.; Banck, M.; James, C. A.; Morley, C.; Vandermeersch, T.; Hutchison, G. R.; *J. Cheminf.* **2011**, *3*, 14. [Crossref]
31. Berman, H. M.; Westbrook, J.; Feng, Z.; Gilliland, G.; Bhat, T. N.; Weissig, H.; Shindyalov, I. N.; Bourne, P. E.; *The Protein Data Bank* **2000**, *28*, 235. [Crossref]
32. Morris, G. M.; Ruth, H.; Lindstrom, W.; Sanner, M. F.; Belew, R. K.; Goodsell, D. S.; Olson, A. J.; *J. Comput. Chem.* **2009**, *30*, 2785. [Crossref]
33. Trott, O.; Olson, A. J.; *J. Comput. Chem.* **2009**, *31*, 461. [Crossref]
34. Cen, Y.; Singh, W.; Wu, Q.; Reetz, M. T.; *Nature Commun.* **2019**, *10*, 3198. [Crossref]
35. Sutherland, J. J.; Nandigam, R. K.; Erickson, J. A.; Vieth, M.; *J. Chem. Inf. Model.* **2007**, *47*, 2293. [Crossref]
36. Altschul, S. F.; Gish, W.; Miller, W.; Myers, E. W.; Lipman, D. J.; *J. Mol. Biol.* **1990**, *215*, 403. [Crossref]
37. López-Gallego, F.; Betancor, L.; Mateo, C.; Hidalgo, A.; Alonso-Morales, N.; Dellamora-Ortiz, G.; Guisán, J. M.; Fernández-Lafuente, R.; *J. Biotechnol.* **2005**, *119*, 70. [Crossref]
38. Migneault, I.; Dartiguenave, C.; Bertrand, M. J.; Waldron, K. C.; *BioTechniques* **2004**, *37*, 802. [Crossref]
39. Freire, R. M.; Ribeiro, T. S.; Vasconcelos, I. F.; Denardin, J. C.; Barros, E. B.; Mele, G.; Carbone, L.; Mazzetto, S. E.; Fechine, P. B. A.; *J. Nanopart. Res.* **2013**, *4*, 1616. [Crossref]
40. Xie, W.; Ma, N.; *Energy Fuels* **2009**, *23*, 1347. [Crossref]
41. Betancor, L.; López-Gallego, F.; Hidalgo, A.; Alonso-Morales, N.; Dellamora-Ortiz, G.; CesarMateo, G. D. O.; Fernández-Lafuente, R.; Guisán, J. M.; *Enzyme Microb. Technol.* **2006**, *39*, 877. [Crossref]
42. Hernández-Fernández, F. J.; de los Ríos, A. P.; Rubio, M.; Gómez, D.; Víllora, G.; *J. Chem. Technol. Biotechnol.***2007**, *82*, 887. [Crossref]
43. Mogensen, J. E.; Sehgal, P.; Otzen, D. E.; *Biochemistry* **2005**, *44*, 1719. [Crossref]
44. Salameh, M. A.; Wiegel, J.; *Open Biochem. J.* **2010**, *4*, 22. [Crossref]
45. Uppenberg, J.; Hansen, M. T.; Patkar, S.; Jones, A.; *Struct. Cell Funct.* **1994**, *2*, 293. [Crossref]
46. Costa, V. M.; de Souza, M. C. M.; Fechine, P. B. A.; Macedo, A. C.; Gonçalves, L. R. B.; *Braz. J. Chem. Eng.* **2016**, *33*, 661. [Crossref]
47. Can, K.; Ozmen, M.; Ersoz, M.; *Colloids Surf., B* **2009**, *71*, 154. [Crossref]
48. Hasan, E.; Manzar, Z.; Haroon, N.; Raza, A.; Ali, S. N.; Lateef, M.; Begum, S.; *RSC Adv.* **2024**, *14*, 36093. [Crossref]
49. Bruce, I. J.; Sen, T.; *Langmuir* **2005**, *21*, 7029. [Crossref]
50. Klapiszewski, Ł.; Zdarta, J.; Antecka, K.; Synoradzki, K.; Siwińska-Stefańska, K.; Moszyński, D.; Jesionowski, T.; *Appl. Surf. Sci.* **2017**, *422*, 94. [Crossref]
51. Kaya, F.; Heitmann Jr., J. A.; Joyce, T. W.; *J. Biotechnol.* **1994**, *36*, 1. [Crossref]
52. Mozhaev, V. V.; Martinek, K.; *Molekulyarnaya Biologiya* **1982**, *16*, 694. [Crossref]
53. Zhang, D. H.; Yuwen, L. X.; Peng, L. J.; *J. Chem.* **2013**, ID 946248. [Crossref]
54. Lish, M. P.; Ashjari, M.; Yousefi, M.; Mohammadi, M.; Ramazani, A.; *Int. J. Biol. Macromol.* **2025**, *297*, 139814. [Crossref]

55. Monteiro, R. R. C.; Andrade Neto, D. M.; Fechine, P. B. A.; Lopes, A. A. S.; Gonçalves, L. R. B.; dos Santos, J. C. S.; de Souza, M. C. M.; Fernandez-Lafuente, R.; *Int. J. Mol. Sci*. **2019**, *20*, 5807. [Crossref]
56. Hu, B.; Pan, J.; Yu, H. L.; Liu, J. W.; Xu, J. H.; *Process Biochem.* **2009**, *44*, 1019. [Crossref]
57. Ferreira, L. F. P.; Mazzi De Oliveira, T.; Toma, S. H.; Toyama, M. M.; Araki, K.; Avanzi, L. H.; *RSC Adv.* **2020**, *10*, 38490. [Crossref]
58. Fernandez-Lafuente, R.; Armisén, P.; Sabuquillo, P.; Fernández-Lorente, G.; Guisán, J. M.; *Chem. Phys. Lipids* **1998**, *93*, 185. [Crossref]
59. Carvalho, P. D. O.; Calafatti, S. A.; Marassi, M.; da Silva, D. M.; Contesini, F. J.; Bizaco, R.; Macedo, G. A.; *Quim. Nova* **2005**, *28*, 614. [Crossref]
60. Almeida, L. C.; Barbosa, M. S.; de Jesus, F. A.; Santos, R. M.; Fricks, A. T.; Freitas, L. S.; Pereira, M. M.; Lima, Á. S.; Soares, C. M. F.; *Biotechnol. Appl. Biochem.* **2021**, *68*, 801. [Crossref]
61. da Fonseca, A. M.; Cavalcante, A. L. G.; Carvalho, R. M. M.; do Amaral, J. F.; Colares, R. P.; Marinho, E. S.; Maia Neto, M.; *Int. J. Res. -GRANTHAALAYAH* **2020**, *8*, 174. [Crossref]
62. Bruice, T. C.; Lightstone, F. C.; *Acc. Chem. Res.* **1999**, *32*, 127. [Crossref]
63. Corici, L.; Pellis, A.; Ferrario, V.; Ebert, C.; Cantone, S.; Gardossi, L.; *Adv. Synth. Catal.* **2015**, *357*, 1763. [Crossref]
64. Fonseca, T. S.; Vega, K. B.; da Silva, M. R.; de Oliveira, M. C. F.; de Lemos, T. L. G.; Contente, M. L.; Molinari, F.; Cespugli, M.; Fortuna, S.; Gardossi, L.; de Mattos, M. C.; *Mol. Catal.* **2020**, *485*, 110819. [Crossref]

*Submitted: June 20, 2025*
*Final version online: January 9, 2026*